UNIVERSITAT POLITÈCNICA DE CATALUNYA
BARCELONATECH
Escola d'Enginyeria de Barcelona Est

FINAL DEGREE PROJECT

Degree in Chemical Engineering

KINETICS OF UO_2 DISSOLUTION UNDER HIGHLY ALKALINE CONDITIONS: APPLICATION OF A THIN FILM CONTINUOUS FLOW-THROUGH REACTOR

Report and Annexes

Author: Narcís Gay Villaret
Supervisor: Ignasi Casas Pons

Call: January 2019

Abstract

The treatment and management of nuclear waste keeps generating technical and ethical problems nowadays, being one of the most important environmental challenges. Due to this problem, international organizations have seen in the concept of deep geological disposal, materialized in Deep Geological Repository (DGR), the most viable and safe way to give a permanent solution to this problem.

Multibarrier containment of DGR will eventually fail, but only tens or thousands of years later may, groundwater be in contact with the spent nuclear fuel (SNF). Said groundwater, is the only likely vector that has the possibility of transporting radioisotopes back to the biosphere. Consequently, SNF itself is the last barrier to offer resistance to the action of water.

In this project, the effect of cementitious waters from the construction of DGR, on the kinetics of dissolution of uranium dioxide (UO_2) has been studied. UO_2 has been used as a chemical analogue of SNF. This type of water leads to highly alkaline conditions with presence of silicate (SiO_3^{2-}) and calcium (Ca^{2+}). Moreover, the influence of carbonate (CO_3^{2}) present in groundwater has been studied. A thin film continuous flow-through reactor system has been used for the quantification of the influence of these compounds on the UO_2 dissolution rate.

The increase of the UO_2 dissolution rate has been studied under basic pH conditions. The decrease produced by the separate influence of SiO_3^{2-}, Ca^{2+} and CO_3^{2-} in different concentrations have been quantified. In addition, several combinations of compounds have been tested and it has been observed that the combined influence of SiO_3^{2-} and Ca^{2+} decreases the kinetics of dissolution of UO_2 in several orders and that CO_3^{2} may inhibit the effects of SiO_3^{2}.

Finally, due to the new tendencies of adding dopants to nuclear fuels, the synthesis and characterization of UO_2 doped pellets has also been done, in this case, the chosen element has been gadolinium (Gd) since its own kinetic study is expected to be carried out in future studies.

The doped pellets have been properly synthesized despite all the technical difficulties encountered. A characterization study has been performed by scanning electron microscopy (SEM) and X-ray diffraction (XRD), which it has determined that the synthesis process requires some improvements.

Resum

El tractament i la gestió definitiva dels residus nuclears segueix generant problemes tècnics i ètics avui en dia, sent un dels reptes mediambientals més importants. En front d'aquest problema, les organitzacions internacionals han vist en el concepte de l'emmagatzematge geològic profund (DGR) la manera més viable i segura d'aïllar i donar una solució final a aquest tipus de residus.

S'espera que transcorreguts milers, o centenars de milers d'anys, el sistema multibarrera que constitueix el DGR sigui degradat per l'aigua subterrània, que entrarà en contacte amb el combustible nuclear gastat (CNG) el qual oferirà la última resistència a ser dissolt i retornat a la biosfera per l'acció de l'aigua.

En aquest projecte s'ha volgut quantificar l'efecte de les aigües de ciment, provinents de la construcció del DGR, sobre la cinètica de dissolució del UO_2, el qual ha sigut utilitzat com a anàleg químic del CNG. El sistema estudiat ha tingut en compte que aquestes aigües porten a condicions altament alcalines amb presència de silicat (SiO_3^{2-}) i calci (Ca^{2+}), com també la influència del carbonat (CO_3^{2-}) present en les aigües subterrànies. Per a la determinació de la influència d'aquests compostos sobre la cinètica de dissolució del UO_2 s'ha utilitzat un sistema de reactor continu de capa fina.

S'ha pogut quantificar com la velocitat de dissolució augmenta en condicions de pH bàsic, així com la disminució produïda en aquesta per la influència separada del SiO_3^2, el Ca^{2+} i el CO_3^{2-} en diferents concentracions. També s'han experimentat diferents combinacions de components, trobant que la influència conjunta de SiO_3^2 i Ca^{2+} disminueixen en varis ordres la cinètica de dissolució i que el CO_3^{2-} podria anular la influència del SiO_3^{2-}.

Per últim, degut a les noves tendències d'afegir dopants als combustibles nuclears també s'ha realitzat la síntesi i caracterització de pastilles d'UO_2 dopades, en aquest cas, amb gadolini (Gd) per a realitzar el seu propi estudi de dissolució en futurs treballs.

Tot i les dificultats tècniques, les pastilles han pogut ser sintetitzades amb èxit. S'ha realitzat una caracterització per microscòpia electrònica de rastreig (SEM) i difracció de raigs X (XRD), en les quals s'ha pogut observar que el procés de fabricació encara requereix d'algunes millores.

Resumen

El tratamiento y la gestión definitiva de los residuos nucleares sigue generando problemas técnicos y éticos hoy en día, siendo uno de los retos medioambientales más importantes. Dado este problema, las organizaciones internacionales han visto en el concepto del almacenamiento geológico profundo (DGR) la manera más viable y segura de dar una solución permanente a este problema.

Se espera que transcurridos miles, o centenares de miles de años, el sistema multibarrera que constituye el DGR sea degradado por las aguas subterráneas, que entraran en contacto con el combustible nuclear gastado (CNG), el cual ofrecerá la última resistencia a ser disuelto y devuelto a la biosfera por acción del agua.

En este proyecto se ha cuantificado el efecto de las aguas de cemento, provenientes de la construcción del DGR, sobre la cinética de disolución del UO_2, el cual ha sido utilizado como análogo químico del CNG. El sistema estudiado ha tenido en cuenta que este tipo de aguas conducen a condiciones altamente alcalinas con presencia de silicato (SiO_3^{2-}) y calcio (Ca^{2+}), como también la influencia del carbonato (CO_3^{2-}) presente en las aguas subterráneas. Para la determinación de la influencia de estos compuestos sobre la cinética de disolución se ha utilizado un sistema de reactor continuo de capa fina.

Se ha podido cuantificar como la velocidad de disolución aumenta en condiciones de pH básico, así como la disminución que producen en esta la influencia separada del SiO_3^2, el Ca^{2+} y el CO_3^{2-} en distintas concentraciones. Además, se ha experimentado con varias combinaciones de componentes y se ha observado que la influencia conjunta del SiO_3^2 y el Ca^{2+} disminuyen en varios ordenes la cinética de disolución del UO_2 y que el CO_3^{2-} podría anular la influencia del SiO_3^{2-}.

Por último, debido a las nuevas tendencias de añadir dopantes a los combustibles nucleares, también se ha realizado la síntesis y caracterización de pastillas de UO_2 dopadas, en este caso, con gadolinio (Gd) para realizar su propio estudio cinético en futuros trabajos.

Las pastillas dopadas han podido ser sintetizadas con éxito pese a todas las dificultades técnicas encontradas. Se ha realizado un estudio de caracterización realizado por microscopia electrónica de barrido (SEM) y difracción de rayos X (XRD), en los cuales se ha podido determinar que el proceso de síntesis requiere algunas mejoras.

Agraïments

En primer lloc, agraeixo al meu tutor, Ignasi, tota l'ajuda, consells i recolzament a la realització d'aquest TFG, una mica més accidentat del que tots hauríem pensat, però que al final com que *no hay mal que por bien no venga* tot serveix per aprendre més. A la Mati per tot el suport i el temps que ha dedicat amb nosaltres al laboratori. I per últim i no menys important, a la Sonia per tota la seva ajuda i el bon ambient de laboratori que s'ha creat durant la realització dels experiments.

També, gràcies a la meva família i amics, en especial a la Núria pels consells anglosaxons.

Summary

1. Introduction

Since the discovery of the radioactivity in the XIX century, the applications of the radioactive isotopes have become an essential element in a variety of fields, not only for energy generation purposes, but also in the industry sector to size thickness and density, in medicine to detect and treat diseases and in art restoration or archaeological dating, among a long list of other uses.

Like any other human activity, it has its consequences: the radioactive waste. The main particularity of this kind of waste is the emission of ionizing radiation. For this reason, it must be isolated from the biosphere. There are two main groups: low level waste (LLW) and intermediate-level short-lived waste (ILW-SL), and high-level waste (HLW). The first group are the vast majority of generated waste and have a short life (Andra, 2018), while the second group is mainly constituted by spent nuclear fuel (SNF) and remains hazardous for hundreds of thousands of years.

An efficient method of waste management is completely necessary for those countries which are using or have been using nuclear power as a source of energy. Many solutions have been proposed since the appearance of the problem, but some of which have been banned. An example of this would be ocean disposal, carried out by some countries for years. Other solutions are too expensive and are not guaranteed to be risk-free, like space disposal, that aims at sending radioactive waste to space. Therefore, deep geological disposal is currently the only permanent disposal solution possible. All countries that use nuclear energy have chosen this option as a safe, permanent mean of managing their radioactive waste in the long term.

The purpose of this final degree project is to investigate the behaviour of a chemical analogue of SNF under representative repository conditions.

1.1. Deep Geological Repository

Deep Geological Repository (DGR) is based on a multibarrier system (Figure 1.1) aiming to isolate the nuclear waste from the effects of human activity or catastrophic events and protect the environment from radiation for hundreds of thousands of years. The purpose of the multibarrier system is to delay the contact of the waste with underground water, which is the only likely vector that may transport radioisotopes back to the biosphere.

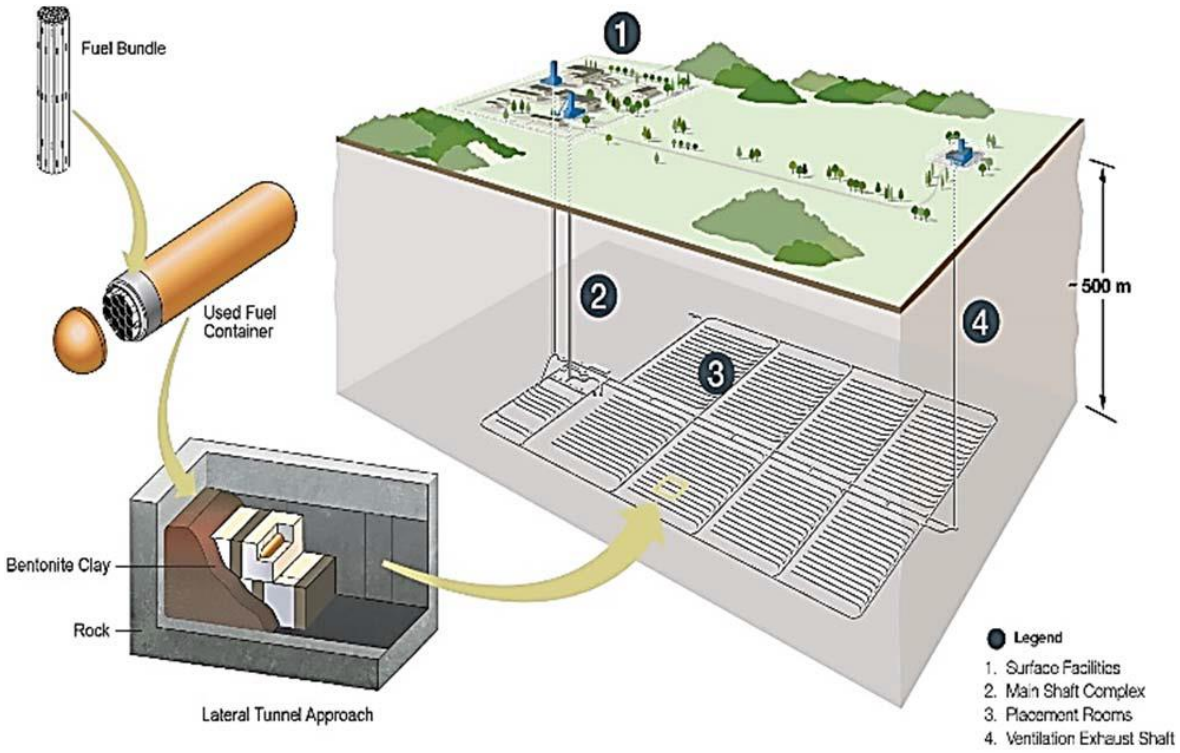

Figure 1.1. Scheme of the DGR facilities and the general scheme of the multibarrier system (Marinceu and Murchison, 2018).

First of all, the geological site itself becomes a barrier and depending on the geological formation, there will be more or less amount of water, and its composition will be different. Therefore, the chosen geological site must have specific characteristics regarding its mechanical stability, thermal conductivity, water permeability, homogeneity and enough thickness to protect the biosphere. Three main types of geological formation are considered to host the repository:

- Granitic: Its stability against the mobility of the land, minimizes the effects of water erosion, but it is impossible to avoid the presence of water currents.
- Salt: Its great elasticity minimizes the effects of possible geological movements. At the same time, it has a minimum quantity of water, but the combination with the salts makes it a very corrosive medium.
- Clay: The terrain minimizes the effects of geological movements but presents a relatively high amount of water. At the same time, the release of the radionuclides (RNs) is very slow in this material since they are adsorbed by clay.

Inside of the repository, the first external barrier is a buffer clay barrier (bentonite). This material will increase the time that water needs to reach the barriers due to its impermeable properties: it increases its volume in contact with water, sealing any possible crack and pore. In addition, the clay barrier might absorb part of the RNs dissolved in groundwater.

The second cladding is the metallic capsule. Several studies are considering which material to use for its construction. Despite titanium and copper alloys have been studied, stainless steel and carbon steel seem to be the most likely options because of technical and economic factors (Azkárate et al. 1999). Its main objective is to contain the SNF, delaying the penetration of water thanks to its resistance to corrosion. At the same time, it avoids physical damage and improves heat transfer.

Even with good engineering control, containment will eventually fail (Savage, 1995) and tens or thousands of years later, groundwater may contact the waste form, so the SNF itself is the last barrier. The UO_2 matrix dissolution will depend on its own chemical composition and the groundwater properties.

Hence, understanding the interactions of the used fuel in a variety of geologic disposal conditions is one of the critical issues to evaluate the safety of different disposal strategies.

1.2. Spent nuclear fuel

Uranium consists mainly of two isotopes: ^{235}U (0.72 atomic %) which is fissile, and ^{238}U (99.27 atomic %) which is fertile. For most commercial reactors, uranium is enriched from 3 to 5% ^{235}U as a low-enriched uranium fuel. In the reactor, the fuel is exposed to a thermal neutron flux that causes two nuclear reactions:

- Fission reaction: produces energy and fission products that give a complex chemistry to SNF. The inventory of radionuclides within the fuel depends on the burn-up (which is a measure of how much energy is extracted from a nuclear fuel and a measure of fuel depletion (*Fuel Burnup*, n.d.) and the linear power rating of the fuel.

$$^{235}U + {}^{1}n_0 \rightarrow \text{fission fragments} + 2\text{-}3 \text{ neutrons} + \text{energy} \quad (1)$$

- Neutron capture and beta decay, which lead to the formation of transuranium elements (Z > 92) of which Pu is the most abundant.

$$^{238}U + {}^{1}n_0 \rightarrow {}^{239}U \rightarrow {}^{239}Np \rightarrow {}^{239}Pu \quad (2)$$

Prior to irradiation, the fuel is uranium as UO_2, although in some countries dopants are added (see Section 1.6). At the end of its useful life in the reactor, about 95% of the spent fuel remains as UO_2. The rest consists of fission products, transuranium elements and activation products. These compounds occur in many different forms, which will form the microstructure of the SNF, as described by Ewing (2015):

1. Fission product gases such as Xe, I and Kr, occur as finely dispersed bubbles in the fuel grains.
2. Metallic fission products like Mo, Tc, Ru, Rh and Pd form immiscible nanometric to micrometric precipitates, called Ɛ-particles.
3. Some fission products like Rb, Cs, Ba and Zr form oxide precipitates.
4. Some fission product elements, such as Sr, Zr, Nb and lanthanides, can form solid solutions with the UO_2
5. Transuranium elements like Pu, can substitute U in the UO_2 matrix.

When following the radial axis of an SNF pellet, three main parts can be distinguished: the gap, the rim and the core of the pellet (Figure 1.2). The distribution changes along the radial axis. Volatile elements such as Cs and I migrate to grain boundaries, fractures and the gap region. The rim zone has high concentrations of ^{239}Pu as a function of the burn-up. And the core is the richest zone in UO_2.

Thus, the SNF has a complex chemistry and phase distribution, which is a result from its thermal history, burn-up and initial composition. All these factors have to be considered when understanding the long term evolution of the fuel and its potential contact with groundwater.

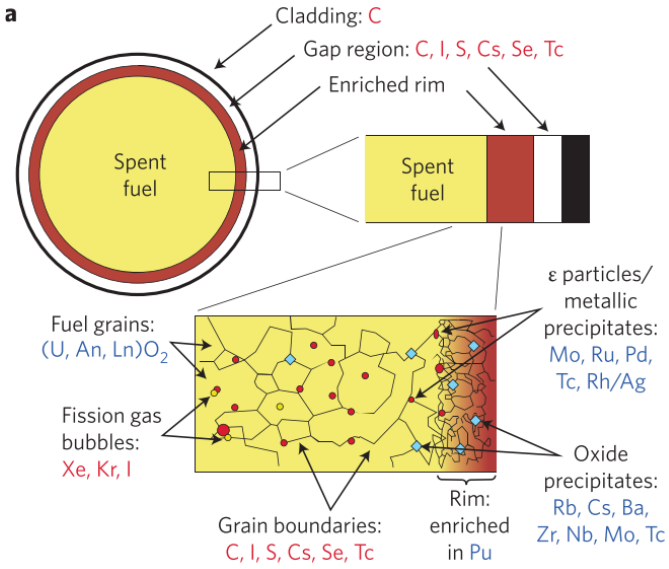

Figure 1.2. Schematic illustration of the microstructure of spent fuel and the distribution of actinides and fission products (Bruno and Ewing, 2006)

Since experimentation with SNF is impossible to do without very specific equipment and many security measures, a simulation of it is necessary. For this reason, regarding that approximately 95% of SNF is UO_2, this compound is used as a representative chemical analogue.

1.3. Mechanisms of dissolution

Once we assume contact of groundwater with the SNF, the dissolution rate and its mechanism become important factors to know in order to predict the release of the RNs. For this reason, it is important to have a good understanding of the dissolution mechanism of a metal oxide as UO_2, and how the water constituents interfere with it.

Two dissolution mechanisms can be distinguished: the diffusion controlled mechanisms, where the dissolution is limited by the rate at which dissolved products are transported to the bulk solution, and the surface controlled mechanisms, based on the concept that detachment from the mineral surface is very slow, limiting the overall reaction rate.

Uranium dioxide dissolution under repository conditions is assumed to be governed by a surface controlled mechanism (Stumm, 1992) that can be schematized as:

1. Fast attachment of reactants to the surface

$$surface\ sites + reactants\ (H^+, OH^-\ or\ ligands) \rightarrow suface\ species \qquad (3)$$

2. Slow detachment of the metal species from the surface of the crystalline lattice into the solution (rate limiting step)

$$suface\ species \rightarrow Me^{n+}(aq) \qquad (4)$$

The dissolution of a mineral is a sum of chemical and physical reaction steps. In the case of a metal oxide, the Me^{n+} in the crystal lattice exchanges its O^{2-} ligands for water or another ligand.

On the one hand. the enhancement of the dissolution rate by a ligand (carbonate groups for example) in a surface-controlled reaction implies that the surface complex formation facilitates the release of ions from the surface to the adjacent solution. On the other hand, the presence of ligands that block surface functional groups may have inhibitory effects that make the dissolution process go slower. The formation of surface films and subsequent phase transformation at the surface modifies its reactivity (Stumm and Wollast, 1990).

1.4. Dissolution and alteration of SNF

1.4.1. Near field conditions

When the other barriers have failed and water reaches the fuel, the alteration and dissolution of SNF begins.

First, there will be an instantaneous release at the time of the waste package failure. Fission gasses such as Xe and Kr and volatile elements like I, Cs, and Cl that have migrated to the grain boundaries and the gap zone will be rapidly released. This fraction of RNs is referred to as the Instant Release Fraction (IRF).

After the first instant release, there will be a much slower long-term release that results from the alteration and dissolution of the fuel matrix. The main processes that affects UO_2 dissolution are illustrated in Figure 1.3. Bruno and Ewing (2006) simplified the SNF alteration as a sequence of four processes.

1. Alpha-radiolysis of water (after 1000 years beta and gamma radiation will be insignificant) breaks the water molecule to produce new species in the system: under reducing conditions creates, oxidizing conditions at the surface of the fuel; under oxidizing conditions its effects are less important. The most stable products created by radiolysis are oxygen and hydrogen peroxide.

$$H_2O + \alpha_{radiation} \rightarrow H_2; O_2; H_2O_2; OH^-; H^+ \quad (5)$$

2. Despite groundwater reducing properties, oxidants produced during radiolysis, or already present in the media, oxidize the UO_2 surface to UO_{2+x} that will contain U(VI). A wide variety of simultaneous processes can take place: H_2 from water radiolysis and Fe^{2+}(aq) from the metal cladding can counterbalance the effect on the oxidation at the fuel surface.
3. The oxidized U(VI) is then dissolved. This dissolution is increased by complexing ligands present in groundwater. Carbonates and oxygen-containing ligands have a strong tendency to form complexes with U(VI).
4. The dissolution of U(VI) eventually continues until saturation, resulting in the precipitation of secondary phases.

Moreover, groundwater constituents will influence the formation of products on the surface of the fuel, which could have several effects (Santos et al. 2006c):

- Block the fuel dissolution process.
- The precipitate phases could incorporate radionuclides released by fuel dissolution, delaying or even preventing their release to groundwater.
- The absorbed α-emitting radionuclides could promote redox conditions and enhance the fuel alteration.

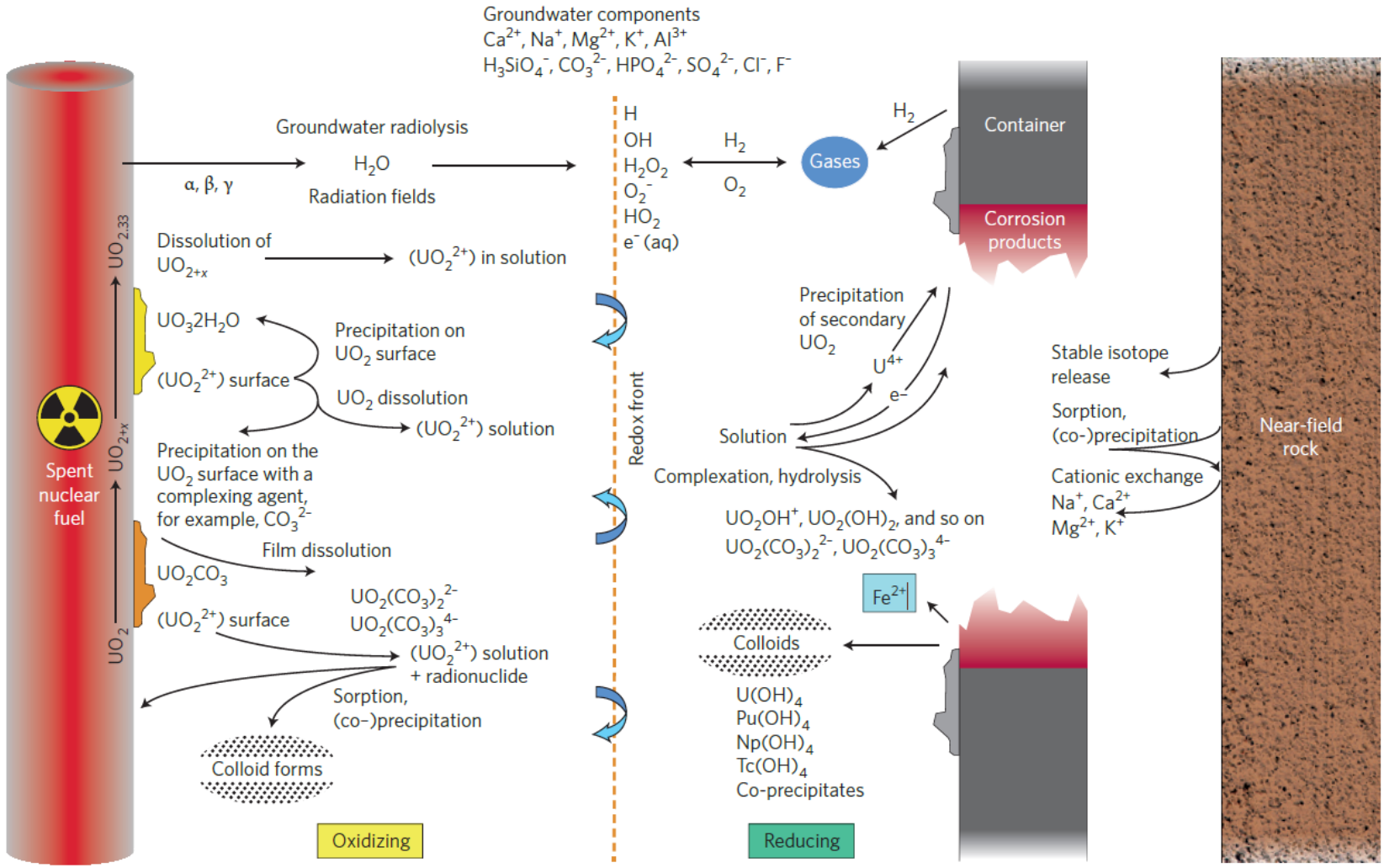

Figure 1.3. Chemical processes that may affect the alteration of spent nuclear fuel in contact with groundwater (Ewing, 2015).

Summing up, after the IRF, the RNs release to the biosphere will be a much slower process of dissolution governed by the own SNF composition and groundwater properties, which will evolve with time. Considering the wide array of situations that can take place in this long process it was decided to focus this work in a particular scenario: the influence of cementitious water.

1.4.2. Redox conditions

The redox potential of the dissolution is one of the most critical variables, since the solubility of UO_2 increases by many orders of magnitude when U(IV) is oxidized to U(VI). Consequently, oxidation is the most important factor that affects UO_2 dissolution. Roth and Jonsson (2008) described the mechanism of oxidative dissolution as:

$$UO_2(s) + OX \rightarrow UO_2^{2+}(s) + RED \quad (6)$$

$$UO_2^{2+}(s) \rightarrow UO_2^{2+}(aq) \quad (7)$$

Since the presence of oxidants is expected, the experiments in this project will be carried out in an oxidative environment.

1.4.3. Cementitious water: silicate and calcium

In view of cement and concrete being used as a structural support in the construction of a DGR (ENRESA, 2014), it becomes necessary to study the interaction of SNF and the groundwater that has been in contact with cement, considering that such contact leads to the development of high alkaline solution containing silicate and calcium ions.

To explain the effect of calcium and silicate it is necessary to present the corrosion two-step mechanism proposed by Santos et al. (2006a) under neutral and alkaline conditions:

$$UO_2 + xH_2O \rightarrow U_{2x}^{V}U_{1-2x}^{IV}O_{2+x} + 2xH^+ + 2xe^- \quad (8)$$

$$U_{2x}^{V}U_{1-2x}^{IV}O_{2+x} + 3OH^- \rightarrow U^{VI}O_{2+x}(OH)_3^- + 2e^- \quad (9)$$

In the recent study performed by Espriu-Gascon et al. (2017) using a SIMFUEL electrode, it can be seen that when SiO_3^{2-} is present, the first step of the reaction is unaffected, but the subsequent oxidation to U^{VI} is slower. The same result was obtained with Ca^{2+}. The first oxidation step is also followed in a normal manner, but it slows down the second step. When both calcium and silicate are present under highly alkaline conditions the surface is stabilized against oxidation to $U^{V}_{2x}U^{IV}_{1-2x}O_{2+x}$. These results are consistent with the conclusions obtained by Santos et al. (2006b and 2006c) that proposed a mechanism to explain this fact:

- Adsorption of Ca^{2+} on the UO_2 surface could supress fuel dissolution either via inhibiting the stabilization of the cation precursor to dissolution $(UO_2(OH)_2)_{ads}$ or by blocking the O^{2-} anion transfer reaction from the fuel surface.
- In the case of silicate, once U(VI) is formed anodically at higher potentials the accumulation of a hydrated U(VI) silicate on the fuel surface occurs, leading to a suppression of anodic dissolution.

In addition, Wilson and Gray (1990) performed several flow-through experiments, where the formation of secondary phases on the fuel surface would not be expected (see Section 1.5.2). The dissolution rate was directly influenced by the presence of calcium and silicate. They observed that the uranium concentration in the effluent decreased by a further factor of 50 with the presence of both species.

Hence, the presence of calcium and silicate, whose origin is in the structural concrete of the repository, leads to high alkaline conditions. At the same time, it is expected that these components decrease the detachment of RNs into the solution.

1.4.4. Effect of pH

The UO_2 dissolution rate, such as its solubility, varies drastically with pH (Figure 1.4). Many studies are carried out in either acid, neutral or slightly alkaline conditions. Few experiments are being performed at highly alkaline conditions.

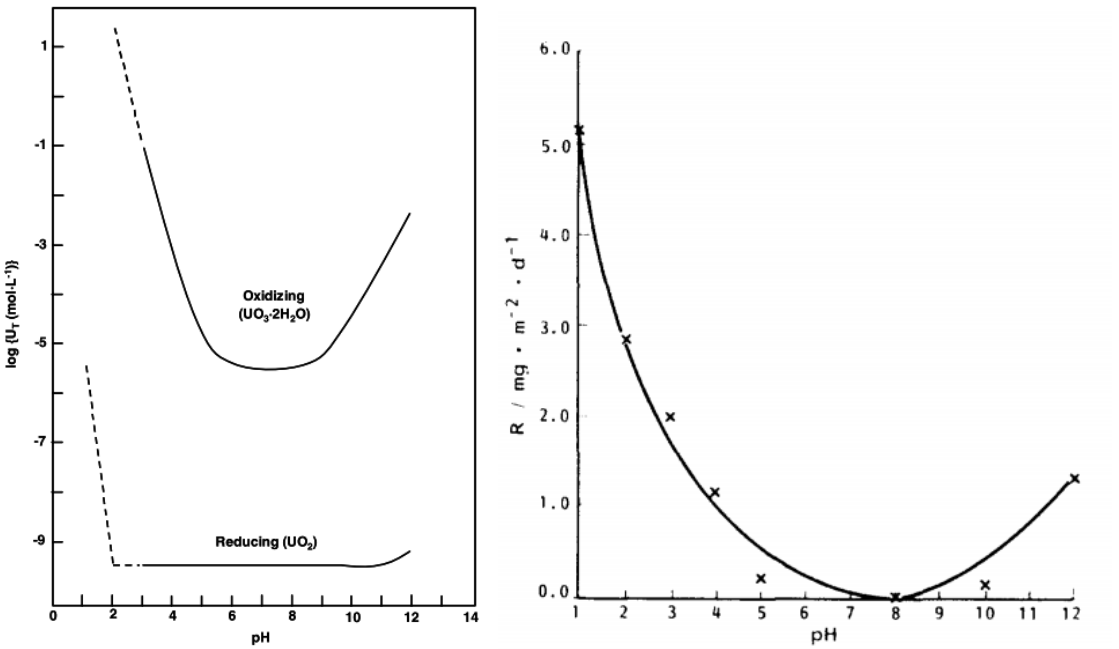

Figure 1.4. (Left) Solubility of uranium dioxide (UO2) and schoepite (UO3·2H2O) as a function of pH at 25 °C. (Right) UO_2 dissolution rate as a function of pH (Thomas and Till, 1984).

Under alkaline conditions, De Pablo et al. (2004) used a three-step mechanism to fit the published corrosion rate data for UO_2 over the pH range 1-12. For pH > 6.8 the proposed mechanism is:

$$> UO_2 + \frac{1}{2}O_2 \leftrightarrow > UO_3 \quad (10)$$

$$> UO_3 + H_2O \rightarrow UO_3 - H_2O \quad (11)$$

$$UO_3 - H_2O \rightarrow UO_2(OH)_2(aq) \quad (12)$$

On the other hand, Santos et al. (2006a) performed electrochemical studies on a SIMFUEL electrode in order to determine the effect of the pH on the corrosion of UO_2. In alkaline conditions the transfer of U(VI) into solution is accelerated by uranyl ion hydrolysis reactions, as uranyl cation is easily complexed by hydroxyl ions in the solution. Then, the general reaction proposed is:

$$UO_2^{2+} + xOH^- \rightarrow UO_2(OH)_x^{(2-x)+} \quad (13)$$

Overall, compared with neutral conditions, at high pH values, the UO_2 dissolution is enhanced. The presence of hydroxyl ions leads to a faster release of cations in the dissolution.

1.4.5. Carbonates

Carbonate is one of the anions present in groundwater and a strong complexing agent of U(VI). Therefore, its influence in contact with the UO_2 has to be studied.

In the study performed by De Pablo et al. (1999), the authors proposed the following mechanisms to describe the influence of the hydrogen carbonate on the UO_2 alteration. Carbonate can't enhance the oxidation but is likely to form complexes with the species present in the solution and in the solid surface. Hence, the first step will be produced by other oxidizing species, probably caused by water radiolysis.

1. Oxidation of the solid surface.

$$> UO_2 + \frac{1}{2}O_2 \leftrightarrow UO_3 \quad (14)$$

2. Surface coordination of U(VI) by HCO_3^-

$$> UO_3 + HCO_3^- \rightarrow > UO_3 - HCO_3^- \quad (15)$$

3. Dissolution of the product species.

$$> UO_3 - HCO_3^- \rightarrow "U(VI)(aq)" \quad (16)$$

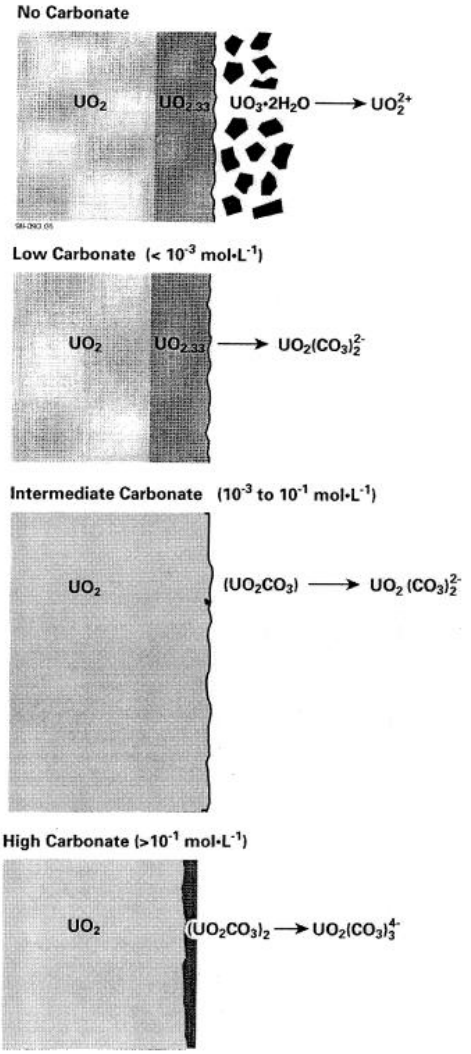

Figure 1.5. Effect of carbonate on UO_2 surface as a function of its concentration (Shoesmith 2000).

This system was also studied by Giménez et al. (2005) and their conclusions agreed with the proposed mechanism, but at relatively low bicarbonate concentrations, lower than 10^{-2} mol·dm^3, a fast detachment of the U(VI) formed in the surface cannot be assumed.

The effect of carbonate was studied in Shoesmith (2000) by electrochemical studies. It was proposed a different alteration mechanism in which the influence of carbonate can be categorized as a function of concentration (Figure 1.5).

- In the absence of carbonate, the formation of uranyl secondary phases can supress the dissolution rate.
- At concentrations of carbonate lower than 10^{-3} mol·dm^3 carbonate increase UO_2^{2+} solubility forming uranyl carbonate complexes in the aqueous phase and the secondary phase precipitation is avoided.
- For intermediate concentrations, 10^{-3} to 10^{-1} mol·dm^3, HCO_3^-/CO_3^{2-} is kinetically involved forming surface intermediates with high solubility, increasing the dissolution rate.
- For higher concentrations than 10^{-1} mol·dm^3 the presence on the surface of uranyl solid phases limit the dissolution rate and the reaction becomes much less dependent on carbonate concentration.

Hence, the presence of carbonate enhances the UO_2 dissolution by means the formation of more soluble complexes. In this project, the experiments will be carried out with intermediate carbonate concentrations, similar to granitic groundwater conditions.

1.5. Determination of the dissolution rate

The goal is to study the kinetics of dissolution of uranium dioxide under hyper alkaline conditions. More specifically, to determine how calcium, silicate and carbonate affect UO_2 dissolution at several different concentrations. The influence will be quantified by means of the dissolution rate (r_{diss}). There are various experimental methods to determine this parameter.

The UO_2 dissolution constitutes a heterogeneous system, since two phases are involved in the reaction, a liquid phase and a solid phase. Due to more than one phase is present, the movement of material from phase to phase must be considered in the rate equation. Thus the rate expression in general will incorporate mass transfer terms in addition to the usual chemical kinetics term. These mass transfer terms are different in type and numbers in the different kinds of heterogeneous systems; hence, no single rate expression has general application (Levenspiel, 1999).

1.5.1. Batch reactors

Dissolution rate can be determined by using a batch reactor. Discontinuous reactors are those where at the beginning of the process the reactants are introduced and do not exchange any matter with its surroundings during the reaction. It is brought to the required pressure and temperature conditions, and it is left to react for a determined time This kind of reactors are widely used and basically consist of a closed tank (Figure 1.6), usually with an agitator.

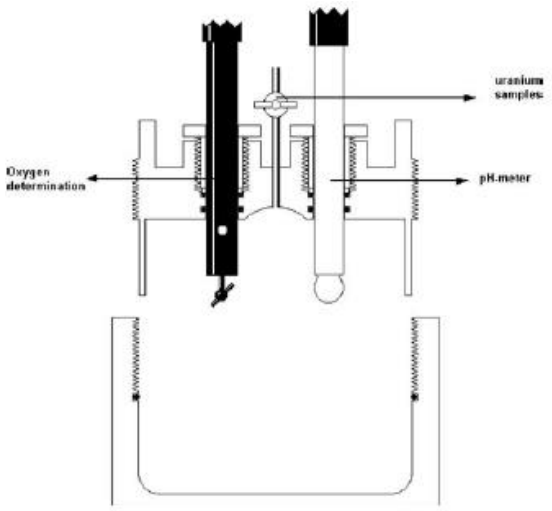

Figure 1.6. Batch reactor used by Giménez et al. (2005) to study the UO2 oxidation and dissolution in bicarbonate media.

Bruno et al. (1991) performed experiments in order to determine separately the influence of pH and HCO_3^- on the dissolution rate. Using a batch reactor containing a defined amount of solid and a solution in which the pH and the oxidation potential was constantly monitored, aliquots for the uranium analysis where taken at certain intervals of time. It was found that the initial values of dissolution could be due to the presence of an oxidized layer UO_{2+x}. Furthermore, the concentrations of the dissolved reactants can easily reach saturation and induce precipitation of secondary phases. Due to the difficulty to avoid the initial oxidized layer, the impossibility to quantify the mass of initial oxidized solid and the formation of secondary phases, it becomes difficult to determine the elementary dissolution rate step with this system. This process limits the increase in concentration of the precipitating elements, which in turn yields an apparent incongruent reaction (Stumm and Wollast, 1990).

1.5.2. Continuous reactors: the thin film reactor

An alternative to batch system are the continuous systems. On a continuous reactor the chemical reaction takes place inside the reactor, which is constantly fed on reactant material at the same time that the products of the reaction are continuously removed, this avoids the undesired secondary phase formation.

Various devices can be used to determine the kinetics and rates of chemical weathering. Flow through columns, fluidized bed reactors and recirculating columns have been used (Figure 1.7). The principle is to achieve a steady state solute concentration in the reactor (Stumm, 1992).

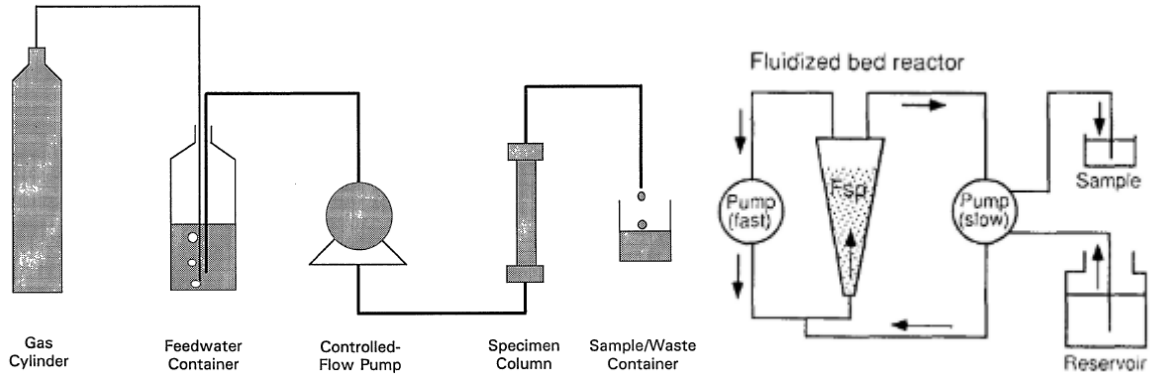

Figure 1.7.Examples of continuous flow-type reactors (Stumm, 1992).

The dissolution rates determined using continuous flow reactors are based on the U(IV) concentration of the effluent at steady state. The amount of U(IV) dissolved depends on the reaction time which is related to the residence time of the solution in the reactor given by:

$$t = V/Q \tag{17}$$

Where V is the volume of solution in contact with the solid phase and Q is the flow rate. The dissolution rate values are calculated using the equation:

$$r_{dis} = Q \cdot [U(IV)] = mol/s \tag{18}$$

[U(IV)] is the uranium concentration of the output solution. The obtained values can be normalized with respect to the total surface area of the solid phase.

$$\frac{r_{dis}}{S} = \frac{mol}{s \cdot m^2} \tag{19}$$

Among the continuous systems, the thin film reactor system is very attractive to determine the UO_2 dissolution rate due to its simplicity and effectiveness (Bruno et al. 1991). Its properties are explained below.

The test solution flows through the reactor where the solid is contained, optimizing the contact between both phases (Figure 1.8) Is pretended to use a layer of solid as thin as possible to minimize diffusion problems as well as to reduce the time of contact between the solid phase and the test solution, since one of the main goals of the system is to keep the solution far from saturation.

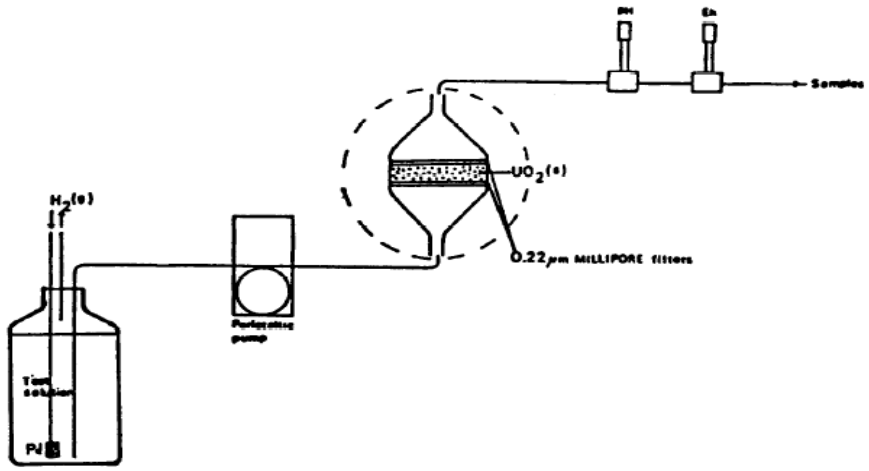

Figure 1.8. Experimental scheme of the thin-film continuous flow reactor used by Bruno et al. (1991).

Once the solid is introduced into the reactor there is no need to manipulate it again, which prevents contaminations by any external agent. The main advantage in front of batch systems is that most soluble and oxidized phases present in the solid are dragged during the first days of experimentation. Once these contributions are eliminated, the effect due only to the bulk solid particles is obtained. Furthermore, the influence of different parameters on the dissolution rate is easily determinable, as only the composition of the input solution must be changed and wait for a new steady state to be reached (Casas, 1989).

In absence of secondary solid phases and if the surface area remains constant, the dissolution rate depends only on the aqueous phase composition. Under these conditions, the system evolves to a steady state and dissolution rates can be determined by multiplying the flow rate Q (dm^3/s) by the concentration of dissolved ion in the output solution.

Furthermore, the possible contributions to the measured reaction rates of either the products of the reaction of the secondary phases formed are avoid because they are dissolved out of the reactor before saturation is reached.

Due to the properties explained above and the fact that this system is able to isolate the elementary UO_2 dissolution reaction from the rest, the rates of dissolution will be determined in this work by using a continuous thin film reactor.

It is important to remark that this system is not pretending to be a simulation of a DGR in failure conditions. In a DGR the groundwater flow will be much slower, and the residence time, much bigger, reaching an equilibrium state in which the precipitation of secondary phases will take place. In this kind of reactor, the products are dragged out of the system by the aqueous phase, before reaching the saturation point, neither products can interact on the results nor secondary phases can be formed by precipitation.

1.6. Doped fuels

To improve the energy production at a lower cost and produce a less quantity of waste are necessities since the beginning of commercial nuclear power generation. As a consequence, several modifications have been introduced, one of them is the utilization of a new generation of doped fuels.

These new fuels, as the undoped ones, at the end of its useful life will be disposed on a DGR. So, it is necessary to know if these additives modify its behaviour with its potential contact with groundwater.

On one hand, dopants such as Gd_2O_3 or Er_2O_3 are used as a burnable absorbers (BA), which means that are materials with a high neutron absorption cross sections, to compensate an excess of reactivity of reactor core (*Burnable Absorbers*, n.d.), this permit to extend the cycle length. However, the use of gadolinium increases the complexity of nuclear design and the fuel manufacture process itself, since the fabrication technique influences the dispersion of Gd within it. Gd oxide and UO_2 have different structures, and this has an effect in most of the physical properties, for instance, on thermal conductivity, the reduction of which leads to higher temperatures in the reactor

Many studies have studied the influence of Gd on the uranium dioxide oxidation (Kim *et al.* 2001; Razdan and Shoesmith, 2013; Liu *et al.* 2017). The main conclusions are that gadolinium slows or even inhibit the oxidative reaction: Gd-doping difficults the accommodation of excess O^{2-} ions when oxidation occurs and also leads to a lattice contraction which reduces the O^{2-} mobility in the UO_2 matrix.

On the other hand, dopants such as Cr_2O_3, Al_2O_3, MgO or Nb_2O_5 are used to improve the fuel performance by enlarging the fuel grain size (Figure 1.9), increasing the fuel density and making a softer pellet. Enlarging the grain size (>30 µm) will extend the length of the diffusion path for fission product gasses to grain boundaries, delaying the gas release. The result of an increased density is augment of ^{235}U mass per fuel assembling which permits longer reactor cycles (Massih, 2014).

Arborelius et al. (2006) performed an study on Cr_2O_3-Al_2O_3-doped fuel (ADOPT) and observed that the final manufactured doped pellets reached higher density and larger grain size than un-doped fuel pellets within a shorter time sintering. The main physical properties including heat capacity, thermal expansion coefficient, melting temperature and thermal diffusivity remain constant. A degradation test

was carried out, and doped fuels presented a reduced rate of fuel washout. Nilsson et al. (2017) performed an oxidative dissolution study of ADOPT pellets, and found that Cr_2O_3 and Al_2O_3 doping has no effect on the matrix dissolution whereas the release of elements from the matrix is delayed by the changes in properties such as densification and grain size.

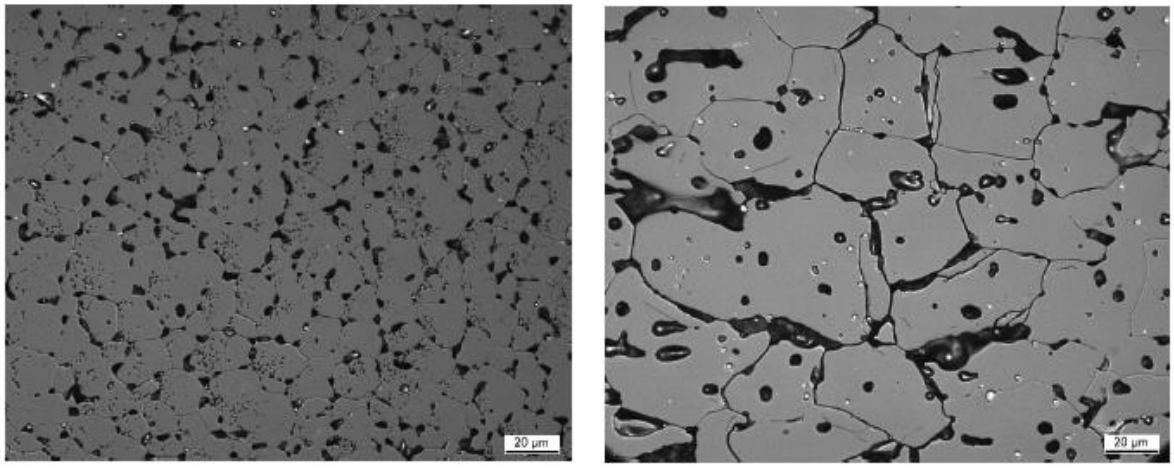

Figure 1.9. Grain size comparison between pure UO_2 pellet (left) and Cr_2O_3-doped pellet (Arborelius *et al.*, 2006).

In this project, the preparation and characterization of Gd doped pellets will be performed. In future works the experimental system studied and developed to determine the kinetics of dissolution of UO_2, will be used to investigate the behaviour of this material.

2. Objectives

Since DGR is the most accepted way to store the SNF a well knowledge of its behaviour under failure conditions is the main objective for researchers. This final degree project wants to contribute in it. The specific objectives are summarized below:

- To assemble, perform and start-up of a thin film flow-through reactor system to determine the kinetics of dissolution of UO_2 under highly alkaline conditions.

- To determine and evaluate the changes in dissolution kinetics under representative repository failure conditions. Determine the effect of calcium, silicate and carbonate on the UO_2 dissolution rate.

- To synthesize and characterise Gd-doped pellets to perform its future dissolution rate study.

3. Experimental

3.1. Test solution and solids

3.1.1. Test solutions

All the solutions were prepared using Milli-Q water (ρ=18.2 MΩ·cm). The pH was adjusted at 12 in all cases by adding NaOH.

Na_2SiO_3 from *Fisher Scientific* was used to prepare 10^{-3}, 10^{-2} and 10^{-1} mol·dm^{-3} of silicate in order to determinate the effect of it on the UO_2 dissolution. $CaCl_2$ from *PanReac* was used to prepare $9.15\cdot10^{-4}$ mol·dm^{-3} solutions to observe how calcium affects to the UO_2 kinetics. Finally, $5\cdot10^{-3}$ and $2.5\cdot10^{-3}$ mol·dm^{-3} solutions of Na_2CO_3 from *PanReac* were prepared to determinate the influence of carbonate.

Different combinations and concentrations were tested in order to determine the combined effects of these compounds. The different combinations experienced are presented in Table 3.1.

Table 3.1. Summary of the conditions of the experimented input solution.

Test solution	pH	[Na_2SiO_3] (mol·dm^{-3})	[$CaCl_2$] (mol·dm^{-3})	[Na_2CO_3] (mol·dm^{-3})
OH^-	12	---	---	---
SiO_3^{2-}	12	10^{-3}	---	---
SiO_3^{2-}	12	10^{-2}	---	---
SiO_3^{2-}	12	10^{-1}	---	---
Ca^{2+}	12	---	$9.15\cdot10^{-4}$	---
CO_3^{2-}	12	---	---	$2.5\cdot10^{-3}$
CO_3^{2-}	12	---	---	$5\cdot10^{-3}$
SiO_3^{2-}- Ca^{2+}	12	10^{-3}	$9.15\cdot10^{-4}$	---
SiO_3^{2-}- CO_3^{2}	12	10^{-3}	---	$5\cdot10^{-3}$
SiO_3^{2-}- CO_3^{2}	12	10^{-2}	---	$5\cdot10^{-3}$
SiO_3^{2-}- CO_3^{2}	12	10^{-1}	---	$5\cdot10^{-3}$
Ca^{2+}- CO_3^{2}	12	---	$9.15\cdot10^{-4}$	$2.5\cdot10^{-3}$
Ca^{2+} - SiO_3^{2-}- CO_3^{2}	12	10^{-2}	$9.15\cdot10^{-4}$	$2.5\cdot10^{-3}$

3.1.2. Solids

ENUSA (Empresa Nacional del Uranio S.A., Spain) provided the synthetic UO_2 used in the study. Supplied as a pellet, it was crushed and sieved to obtain powder. Different particle sizes were obtained. Ranging from 300 to 100 µm to study the kinetics of dissolution and 20 to 10 µm for the preparation of Gd-doped pellets.

Gadolinium oxide from *Sigma Aldritch* was mixed with UO_2 to prepare the 10 mol% Gd-doped pellets.

3.2. Methodology

3.2.1. Kinetics of dissolution

As explained in 1.5.2, one of the characteristics of the thin film reactor system is its simplicity. The dissolution was pumped by means of a peristaltic pump through the reactor, where the solid was contained. The effluent was disposed in the waste bottle unless a sample wanted to be collected in order to analyse the uranium concentration.

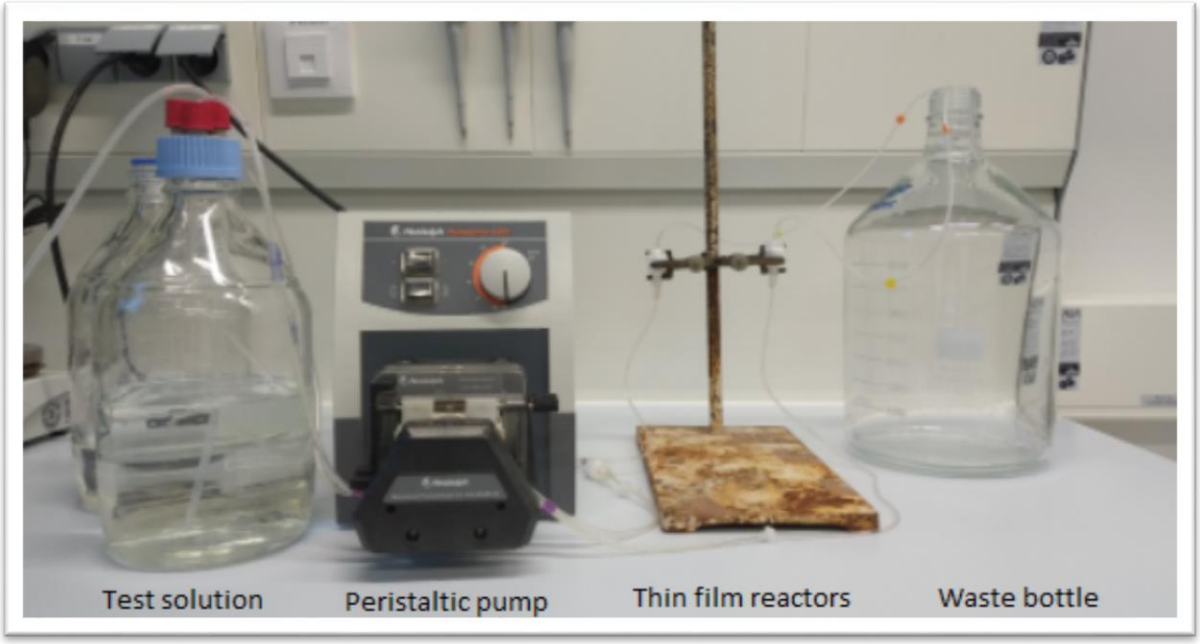

Figure 3.1. Picture of the experimental system.

As shown in Figure 3.1, the test solution was pumped from a bottle to minimize contaminations. In those experiments where calcium was used, a stream of nitrogen was pumped constantly into the bottle to avoid reactions with air, which leads to a formation of calcium carbonate precipitates.

To streamline the process, six reactors were settle up at the same time. The solid was contained into the reactor between two 0.22 µm Millipore filters. The minimum possible quantity of UO_2, only a thin layer of solid, was introduced within each reactor. It was observed that the necessary amount ranged from 0.15 g to 0.20 g.

To be able to compare the results of different reactors it was necessary to normalize the obtained values. Consequently, the introduced mass and the specific surface area of UO_2 must be known with exactitude.

The specific surface area, is directly related with the particle diameter and the porosity. The dissolution rate depends strongly on this parameter: since UO_2 is not a porous substance, the smaller the particle, the bigger the specific surface area. This means that there will be more contact surface between the solution and the solid, and thus an increased fraction of the solid will be dissolved.

In this project, initially a particle size of 50-75 µm was used, but this diameter presented problems with flow rate and was changed to 100-300 µm following the indications of other articles (Casas *et al.*, 1994; De Pablo *et al.*, 1999). The values of the specific surface area of UO_2 used in this project were determined in Torrero (1995) by using Brunauer, Emett and Teller (B.E.T) method, which consists on the adsorption of a gas by the studied solid. The specific surface area for particle diameters ranging from 100 to 300 µm is $1.13 \cdot 10^{-2}$ $m^2 \cdot g^{-1}$.

Once the system was up and running, samples were taken periodically. The initial samples were interesting as they illustrate the dragged out of the oxidized phases, which demonstrate the evolution to a stationary state. After this "cleaning" process, new steady states were reached faster. To evaluate the influence of a different compound on the UO_2 kinetics it was necessary to change the input test solution and wait for a new steady state. Once this state was achieved, to determine the dissolution rate was possible.

The sample collection process was as follows: For a fixed period of time the effluent was collected into a previously weighted test tube. Then, knowing the posterior weight and assuming that the density of the dissolution was 1 $kg \cdot dm^{-3}$, the flowrate Q could be calculated. Finally, 1 mL of the sample was diluted into 4 mL of HNO_3 2% and then 1 mL of dissolution HNO_3 65% was added to acidify it.

Finally, the uranium concentration of the samples was analysed by ICP-MS (see Section 3.3.1). The last step was to calculate dissolution rate as a product of flowrate and uranium concentration by means of Equation (18) and normalized by Equation (19)

3.2.2. Doped samples

The followed synthesis method was inspired by the one used by Baena et al. (2015). There are various methods to synthetize Gd-doped pellets, but the route that was followed in this project was the mechanic blend. This is because of its simplicity and the fact that is the one used by the nuclear fuel manufacturers (IAEA, 1995). The different parts of the method are explained below. The flowsheet of the process can be seen in Figure 3.2.

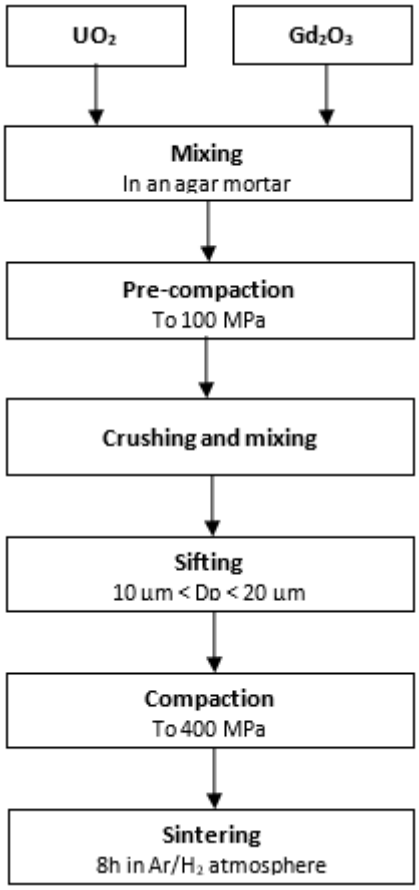

Figure 3.2. Flowsheet of the Gd-doped sintering method, modified from Baena et al. (2015).

Two types of pellets were prepared: pure UO_2 pellets to use as a control, and doped UO_2 pellets with 10 mol% Gd_2O_3 to determinate the influence of Gd.

First of all, the required masses of uranium dioxide and gadolinium oxide powder were mixed in an agar mortar. To improve the blend between the solids, the mixture was pre-compacted to 100 MPa in the press. The resulting pellet was crushed and mixed again. After that, it was sifted to a particle diameter ranging from 10 to 20 µm. Finally, a final compaction to 400 MPa in the press was performed. The pellets had a thickness[1] of 0.5 mm and a diameter of 13 mm, which was set by the internal diameter of the press.

The last step of the process was the sintering of the pellet. The objective is to obtain a solid solution constituted by a solid phase of uranium and gadolinium. The sintering process was carried out in a

[1] These experiments are part of a thesis whose one of the objectives is to observe the oxidation of the Gd-doped pellets under different conditions in order to analyse the influence of Gd in the SNF alteration. This study will be carried out into a XPS, where the thickness of the input sample cannot be much bigger than 5 mm.

horizontal tube furnace ST196030 HG from *Hobersal* for 8 h at 1750 °C in an argon atmosphere with 5 vol% hydrogen in order to prevent the oxidation of U(IV) to U(VI). Due to its extreme temperatures, the joints were constantly refrigerated with a flow of water, as seen in Figure 3.3.

Figure 3.3. Horizontal tube furnace ST196030 HG from Hobersal, capable to reach 1900 °C.

3.3. Analytical techniques

3.3.1. Inductively Coupled Plasma Mass Spectroscopy

Inductively coupled plasma mass spectroscopy (ICP-MS) technique is highly sensitive and able to quantitatively determine almost all the elements in the periodic table at very low concentrations (ppb and ppt). It is based on the coupling of a method to generate ions (inductively coupled plasma) and a method to separate and detect the ions (mass spectrometer).

The sample, in liquid form, is transported by means of a peristaltic pump to the nebulizer system where it is transformed into an aerosol thanks to the action of argon gas. Then, it is conducted to the ionization zone (Figure 3.4) consisting of a plasma generated by subjecting a flow of argon gas to the action of an oscillating magnetic field induced by a high frequency current. In the interior of the plasma temperatures of up to 8000 K can be reached. Under these conditions, the atoms present in the sample are ionized. The ions pass into the quadrupole filter through an increasing vacuum interface, there they are separated according to their charge/mass ratio. Each of the tuned masses reaches the detector where its abundance in the sample is evaluated (Skoog, et al. 2008).

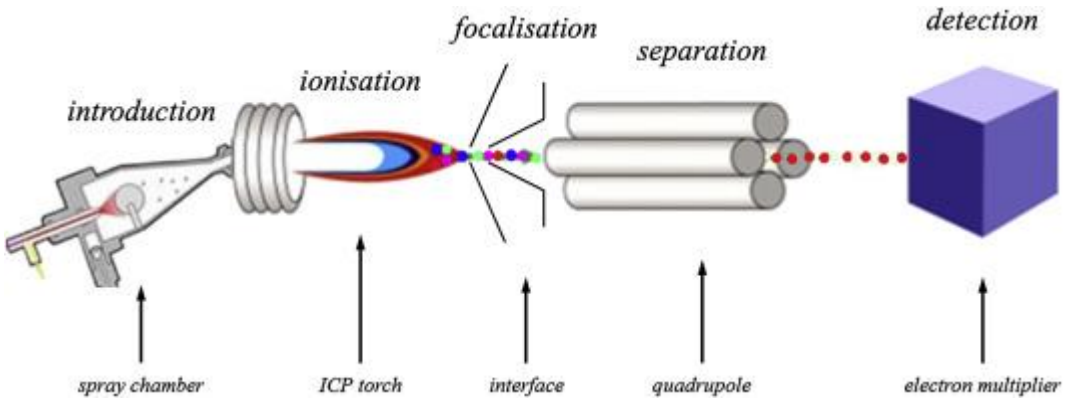

Figure 3.4. Scheme of an IPS-MS system from Aceto (2016).

The device used to determine the uranium concentration was an ICP-MS 7800 from Agilent Technologies® (Figure 3.5) available at *Centre de Recerca en ciència I Enginyeria Multiescala de Barcelona (CRnE)*.

The use of ICP-MS had some requirements: it took the samples in liquid form into plastic 10 mL test tubes and the concentration of salts had to be less than 0.1%: this is why, they were diluted in 1:5 proportion in HNO_3 2 %vol.

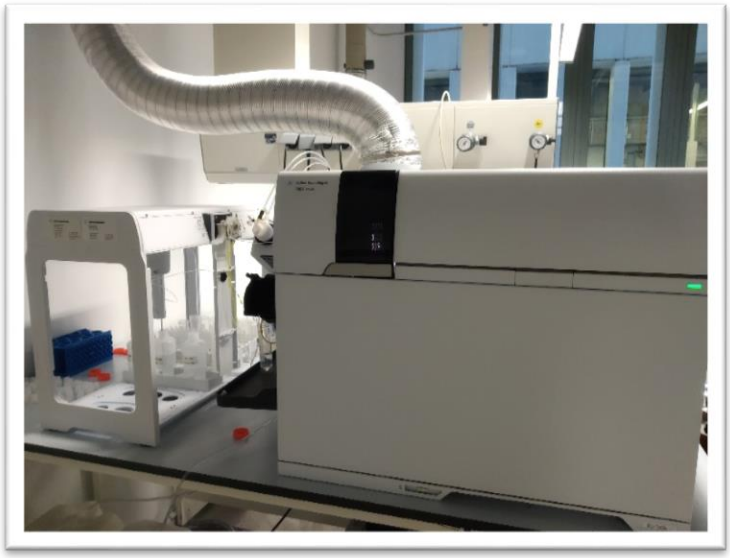

Figure 3.5. ICP-MS 7800 from Agilent Technologies at the CRnE (UPC)

3.3.2. Scanning Electron Microscope

Scanning Electron Microscope (SEM) is a technique used for the quantitative and qualitative structure of microstructured materials. An image obtained by SEM is constructed by a focused electron beam that scans the surface of a sample. This implies a higher resolution and a better depth with respect to

optical microscopes, since the wavelength of an electron beam is much smaller than light (Zhou *et al.*, 2007).

Different interactions are produced between the electron beam and the surface (Figure 3.6). For each interaction, there is a type of detector that provides specific information of the sample analysed

The production of secondary electrons (SE). which are the electrons reflected directly by the action of the incident ray, gives information regarding the topography and morphology of the sample. The backscattered electrons (BSE) are the product of a deeper interaction with the sample, whose interaction with the atoms give compositional qualitative information of the analysed specimen. The excited atoms by the incident beam emit X-rays, by means of an X-ray diffraction spectroscopy detector (EDS) it is obtained an elemental analysis of the sample.

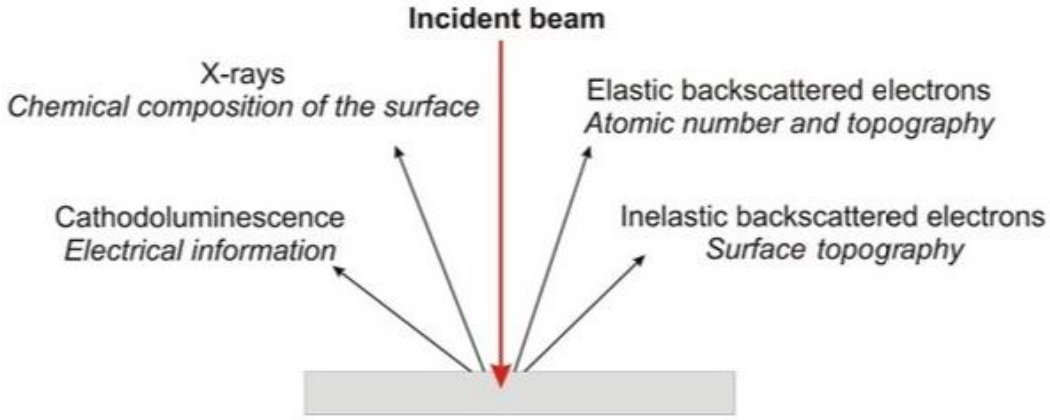

Figure 3.6. Signals generated by the electron beam-specimen interaction in the scanning electron microscope and the regions from which the signals can be detected (Zhou *et al.*, 2007).

SEM analysis and Energy Dispersive Spectrometry (EDS) tests were performed using a *Phenom XL* from *PhenomWorld* (Figure 3.7 A) equipped with a secondary and backscattered electron detector and an energy dispersive X-ray detector. The accelerating voltage was 15 kV.

The samples were placed on a metal support (Figure 3.7 B). Any coating was needed due to the uranium semiconductor properties.

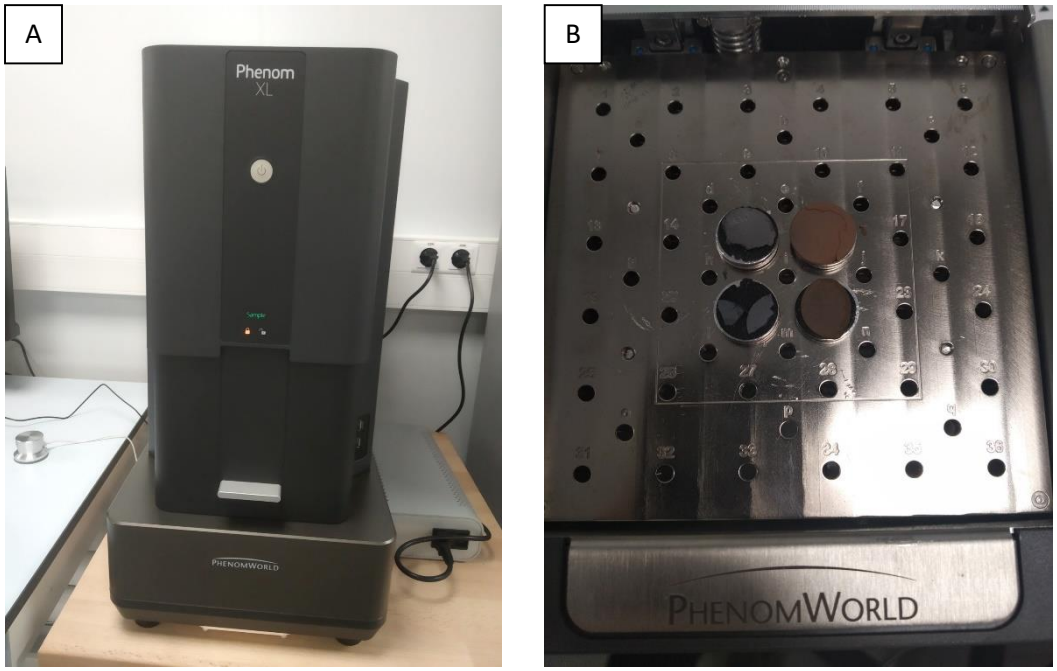

Figure 3.7. A. Picture of the SEM available at the CRnE. B. Preparation of the samples.

3.3.3. X-Ray Diffraction

X-Ray powder Diffraction (XRD) is a basic characterization technique for all those substances with crystalline structure. This technique, such as SEM, is non-destructive, which allows the recovery of the material studied.

It is widely used in the sectors of mineralogy and materials engineering, especially in metallurgy and ceramics. Among its uses are: determination of the purity of the samples, quantitative analysis of a compound within a material, identification of phases, and determination of phase diagrams as well as the determination of crystalline structures.

X-rays are produced when an electrically charged particle with sufficient kinetic energy is quickly stopped. Electrons are the commonly used particles and radiation is obtained in a device known as an X-ray tube.

Diffraction of X-ray occurs when an X-ray beam, with a determined wavelength, interacts with a crystalline substance. X-ray diffraction is based on the coherent dispersion of the X-ray beam in contact with matter and the constructive interference of waves that are in phase, which are dispersed in certain directions of the space. The constructive interference gives peaks of intensity in determined angles associated to distances between crystalline plans (Birkholz, 2006).

The diffraction phenomenon is described by means of Bragg's law (Equation 4.2), which predicts the direction in which constructive interference occurs between X-ray beams scattered coherently by a crystal:

$$n\lambda = 2dsin\theta \tag{20}$$

The radiation produced by the diffraction can be detected with an automatic diffractometer (Figure 3.8), that is, an X-ray detector that records the angles between which the incident X-ray beam has been diffracted.

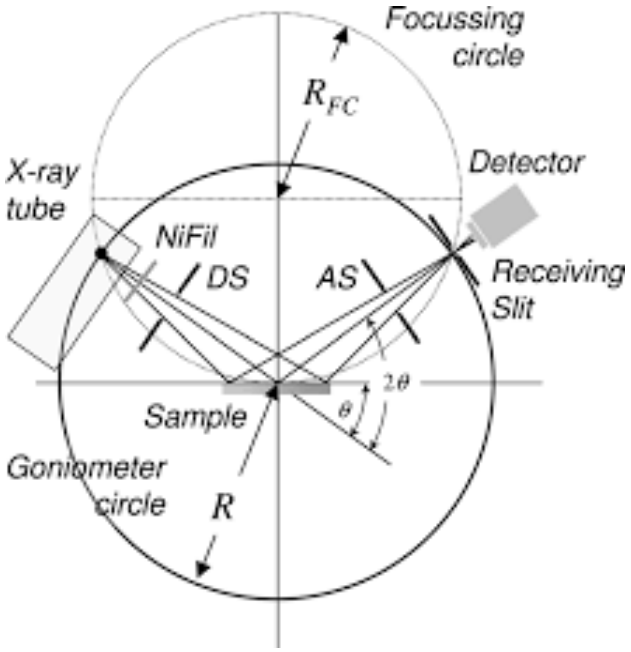

Figure 3.8. Schematic representation of ϑ/2 ϑ diffraction in Bragg-Bentano geometry (Birkholz, 2006)..

Thus, the intensity of the diffracted beam depends on the geometric arrangement of the atoms and the class of atoms present. This causes each crystalline substance to present its own diffraction spectrum, which is an authentic "fingerprint" of each substance, allowing its identification in any mixture where it is present.

XRD analysis was performed with a D8 Advance diffractometer from *Bruker* (Figure 3.9) provided with a Cu LFF tube (Cu Ka1 = 1.54059 Å) and operated in Bragg–Brentano parafocusing geometry, θ-θ configuration and Göbel converging mirrors. Due to the small amount of sample, the scan was performed on capillary tube. Diffractograms were acquired over the range 27–143°. The used step size was 0.004° and 1 s per step.

Figure 3.9. D8 Advance diffractometer from Bruker available at CRnE.

The sample was taken as fine powder with a particle size smaller than 50 µm in order to analise it by cappilary method.

4. Results and discussion

4.1. Alkaline conditions

The first experiments were carried out in alkaline conditions without the effect of any other compound in order to determine the dissolution rate at pH 12. Samples were collected since the first moment to observe how the oxidized species were dragged out of the system. In Figure 4.1 and Figure 4.2 this phenomenon can be observed. During the first hours, uranium concentration in the effluent reached values higher than 2000 ppb, while after the first 48 h, the output concentration decreased to values lesser than 500 ppb, thus reaching the steady state.

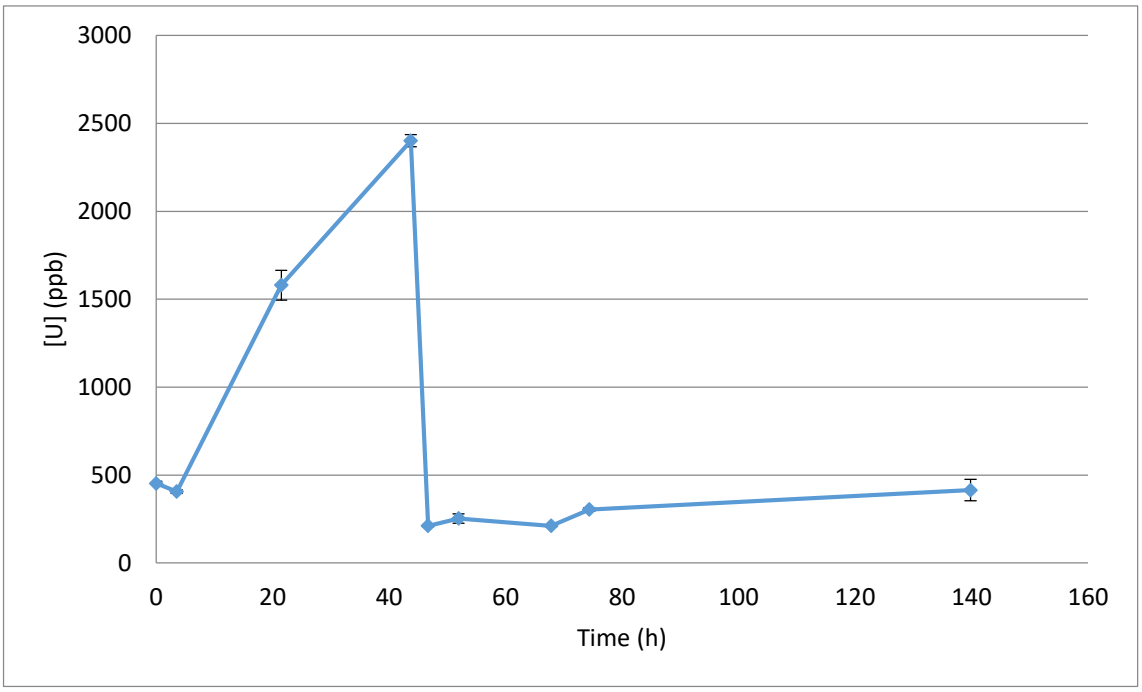

Figure 4.1. Uranium concentration obtained at pH 12 on the effluent solution.

The U concentration should be constant while in steady state but, as the figure above shows it is increasing. This is because of problems with the experimental system: the flow rate decreased slowly with time. Despite this variation, results are consistent, as the flow is lower more uranium is dissolved. In Figure 4.2 it can be seen that the dissolution rate is practically unaffected.

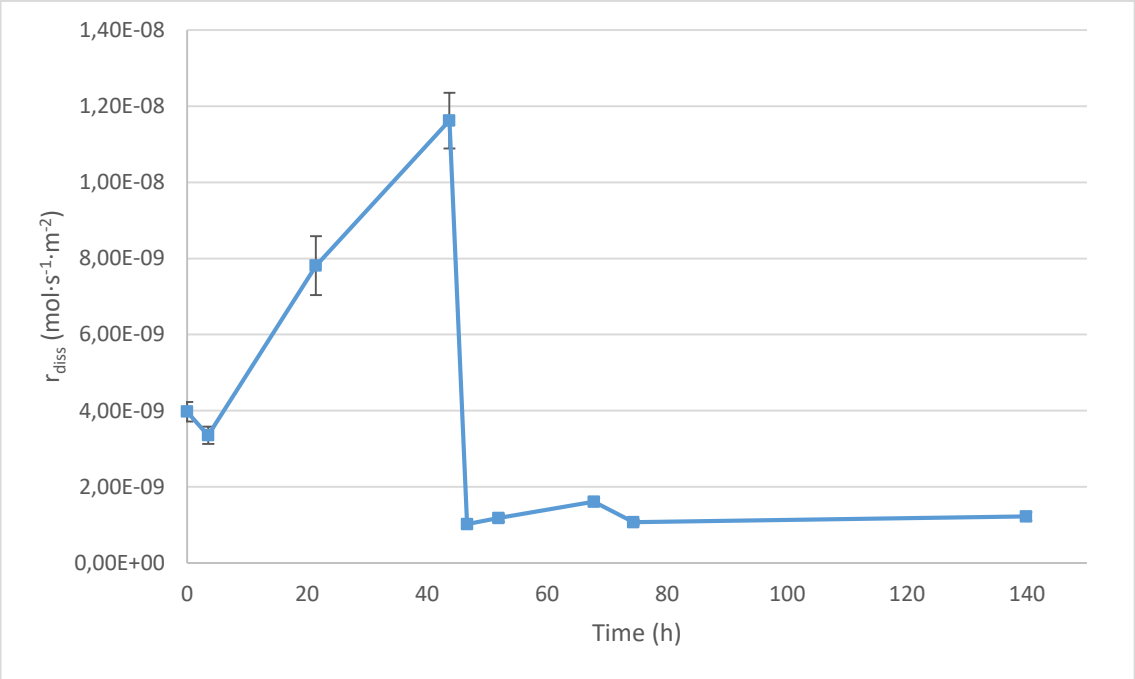

Figure 4.2. Dissolution rate obtained at pH 12 since the settled up of the system.

From the previous figure, taking into consideration only the measures once the stationary state has been reached, it can be concluded that the dissolution kinetics of UO_2 at pH = 12 are:

$$pH = 12 \rightarrow r_{diss} = (1.20 \pm 0.16) \cdot 10^{-9} \frac{mol}{s \cdot m^2}$$

This kinetic value will be the one of reference to compare the influence of the different compounds.

In order to compare this value, a bibliographic research has been done. Few kinetic experiments have been performed at highly alkaline conditions. Thomas and Till (1984) performed batch experiments to determine the influence of pH on unirradiated UO_2 kinetics. They obtained a dissolution rate equal to $6.43 \cdot 10^{-11}$, about 20 times lower than the one obtained in this project. It is difficult to compare both values due to the formation of solid phases that may occur in batch experiments.

De Pablo et al. (2004) also studied the dependence of pH on UO_2 and developed a model to predict the dissolution rate (Figure 4.3). Once again, the obtained value cannot be verified because the model does not consider values at a pH higher than 12. Furthermore, it falls in contradiction with Thomas and Till (1984) because they found that dissolution rate increases at higher pH (Figure 1.4). In disagreement with the proposed model, corrosion studies performed by Espriu-Gascon (2017) found that the corrosion process was enhanced at pH 12.

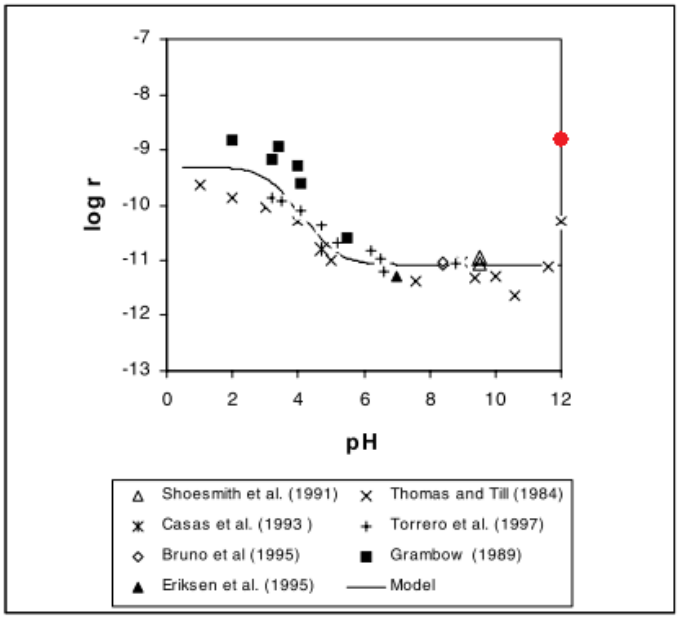

Figure 4.3. Comparison of the predicted values with data from literature (De Pablo et al. 2004). Marked in red, the obtained value in this work.

In conclusion, it seems that UO_2 dissolution rate increases at high pH values, which could indicate a promoted dissolution at high OH^- concentrations. The obtained dissolution rate is consistent with the results of the subsequent sections.

4.2. Influence of calcium, silicate and carbonate

In this section, the separate effects of silicate, calcium and carbonate on the UO_2 kinetics will be discussed. The combined effect of distinct compounds will be discussed in the next section. All the experiments were carried out at pH 12 to be able to make relevant comparisons.

First of all, it should be noted that from now on, to make possible comparisons, the initial time is considered as the moment when the steady state has already been reached. To facilitate visualization, the dissolution rate is delimited by the upper and lower limit of uncertainty and the obtained experimental data are the represented points.

In some of the following cases, data of the same steady state presents certain dispersion. They have been accepted and may be due to some of the experimental problems that have been encountered. In many cases, it was difficult to maintain a constant flow rate due to solid compaction. In other experiments, especially those with high concentrations, precipitates were formed in the test solution and probably induced errors. Moreover, some tests had to finish sooner that planned due to ruptures of the peristaltic pump tubes.

The obtained results from the experimentation with a test solution containing $9.15 \cdot 10^{-4}$ M of **Ca^{2+}** are shown in Figure 4.4.

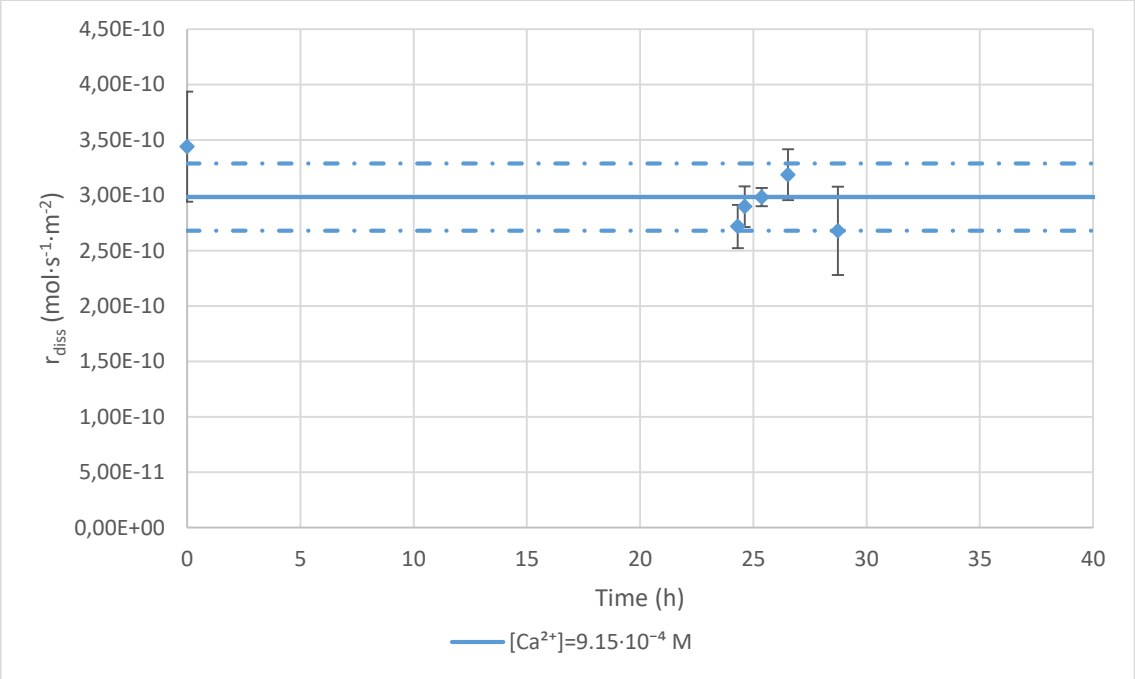

Figure 4.4. Dissolution rate obtained testing an input solution of $9.15 \cdot 10^{-4}$ M of Ca^{2+}.

The dissolution rate for UO_2 with presence of $9.15 \cdot 10^{-4}$ M of calcium is:

$$pH = 12; [Ca^{2+}] = 9.15 \cdot 10^{-4} M \rightarrow r_{diss} = (2.98 \pm 0.30) \cdot 10^{-10} \frac{mol}{s \cdot m^2}$$

As expected for similar experiments performed by Wilson and Gray (1990), with presence of calcium in the solution, the UO_2 dissolution rate is decreased by a factor nearly of 4.

Figure 4.5 illustrates the kinetics obtained with presence of 10^{-3}, 10^{-2} and 10^{-1} M of **SiO_3^{2-}**.

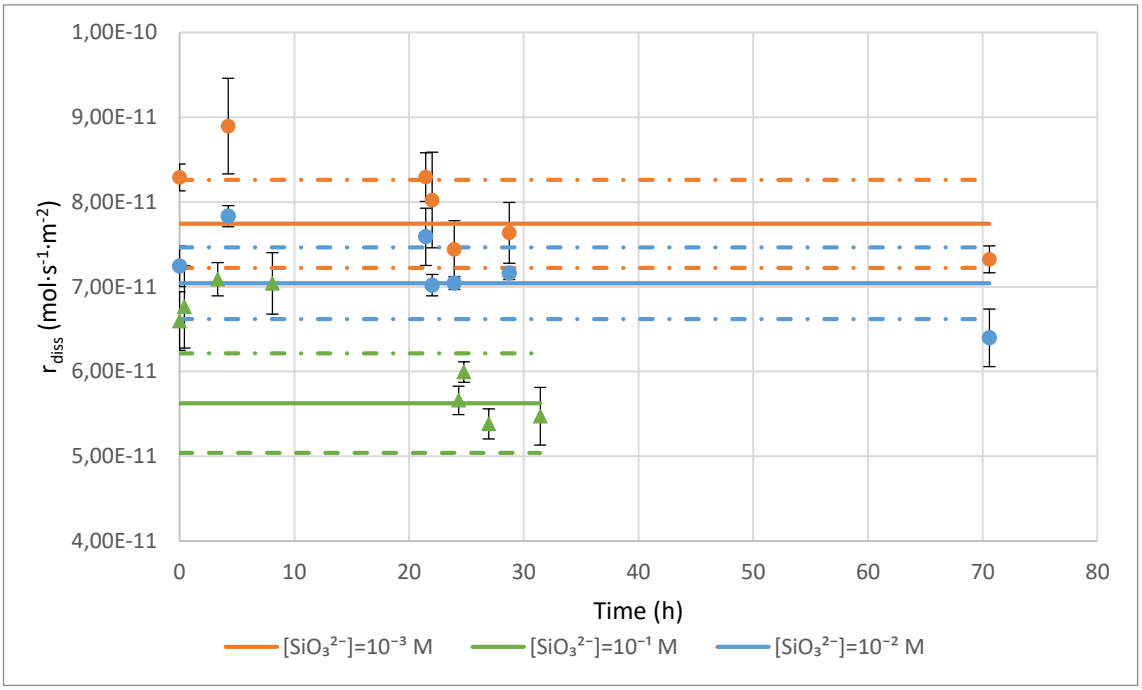

Figure 4.5. Dissolution rate obtained testing input solutions of 10^{-3}, 10^{-2} and 10^{-1} M of SiO_3^{2-}.

Although in these cases the attainment of steady state showed a large scattering, a clear trend can be distinguished: the dissolution kinetics decrease as the silicate concentration increases. It should be noted that despite increasing the concentration of SiO_3^{2-} several orders, the kinetics only makes a small decrease. SiO_3^{2-}, like Ca^{2+}, blocks the process of dissolution but indicates a much stronger influence on this suppression.

The obtained kinetics values are:

$$pH = 12; [SiO_3^{2-}] = 10^{-3} M \rightarrow r_{diss} = (7.74 \pm 0.52) \cdot 10^{-11} \frac{mol}{s \cdot m^2}$$

$$pH = 12; [SiO_3^{2-}] = 10^{-2} M \rightarrow r_{diss} = (7.04 \pm 0.42) \cdot 10^{-11} \frac{mol}{s \cdot m^2}$$

$$pH = 12; [SiO_3^{2-}] = 10^{-1} M \rightarrow r_{diss} = (5.63 \pm 0.59) \cdot 10^{-11} \frac{mol}{s \cdot m^2}$$

Results obtained from experimentation with $2.5 \cdot 10^{-3}$ and $5 \cdot 10^{-3}$ M of **CO_3^{2-}** are presented in Figure 4.6.

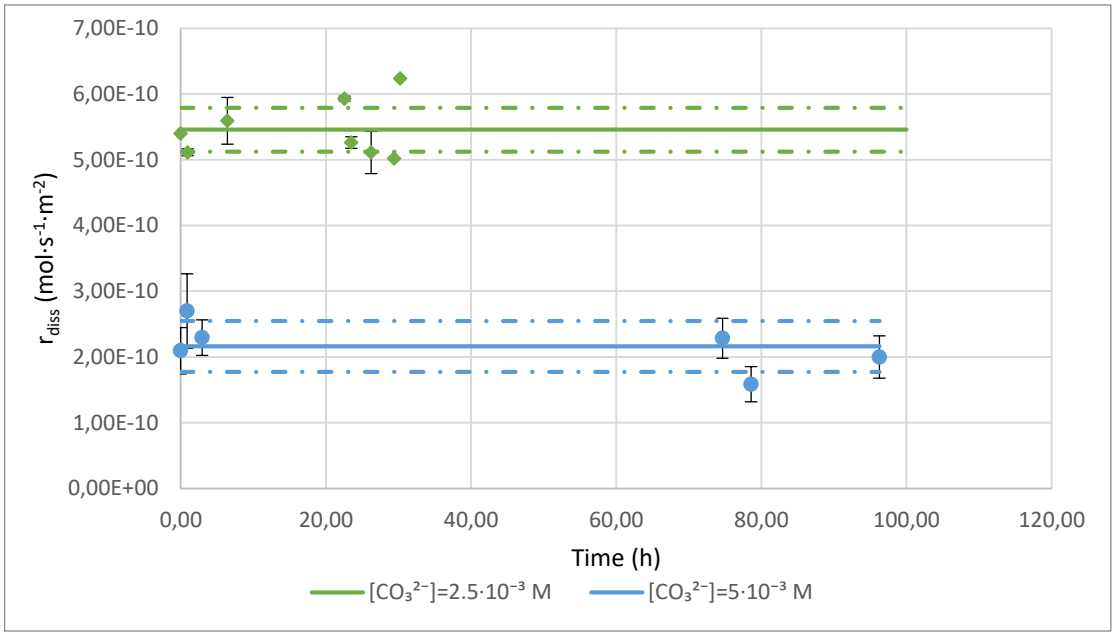

Figure 4.6. Dissolution rate obtained testing input solutions of $2.5{\cdot}10^{-3}$ and $5{\cdot}10^{-3}$ M of CO_3^{2-}.

The obtained kinetics values are:

$$pH = 12; [CO_3^{2-}] = 2{,}5 \cdot 10^{-3} M \rightarrow r_{diss} = (5.46 \pm 0.52) \cdot 10^{-10} \frac{mol}{s \cdot m^2}$$

$$pH = 12; [CO_3^{2-}] = 5 \cdot 10^{-3} M \rightarrow r_{diss} = (2.16 \pm 0.37) \cdot 10^{-10} \frac{mol}{s \cdot m^2}$$

In the case of carbonate, the effect is contrary to the one expected. The dissolution kinetics, instead of being faster, as anticipated by other experiments, are actually slow down. The results show that the dissolution rate decreases as the carbonate concentration increases. The results that have been obtained, however, are inconsistent with other investigations. Further investigations will be performed in the future, since few experimentation has been performed in these conditions in highly alkaline conditions.

Finally, in Figure 4.7 the obtained kinetics for each compound are compared. Due to different orders of magnitude, the comparison of the results is made possible thanks to the logarithmic scale. Furthermore, instead of representing the values, with its confidence interval, like in the previous graphs, only the experimental data is represented, in attempt to facilitate visualization.

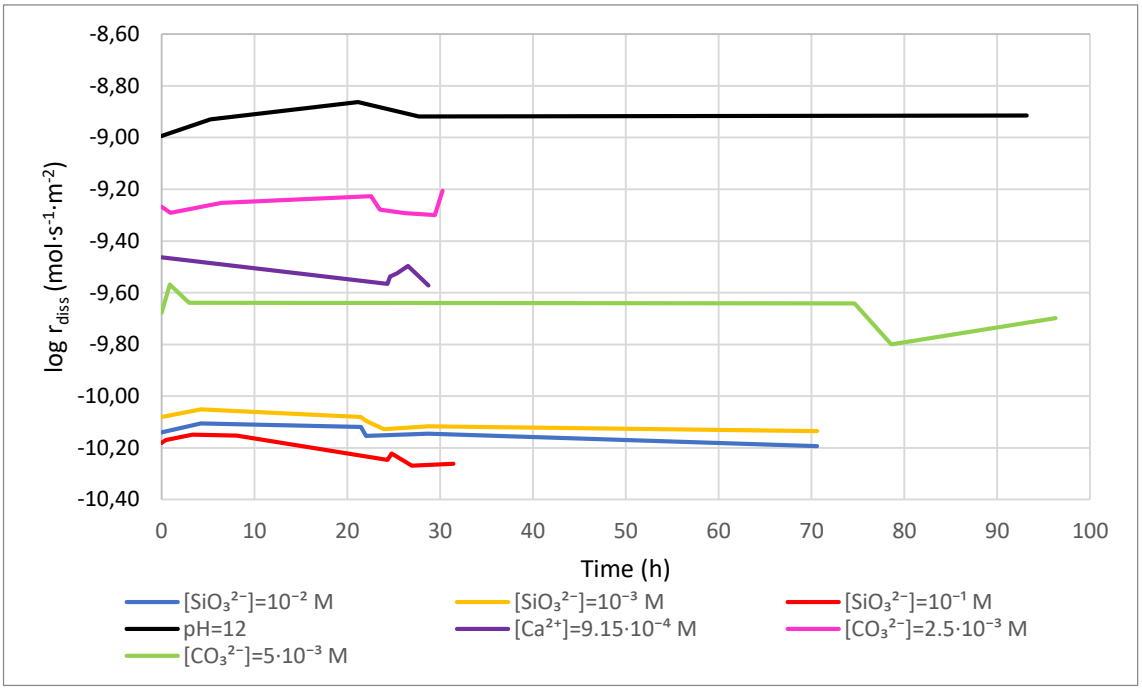

Figure 4.7. Comparison of the obtained dissolution rates.

Thanks to the overall vision of the graph, the effect on the kinetics of the various components is easily compared. As expected, the effect of silicate on kinetics is much more pronounced than that caused by calcium. Moreover, the dissolution rate decreases as SiO_3^{2-} concentration increases. Also, as mentioned, the addition of carbonate decreases dissolution kinetics. Unexpectedly, the effect on the UO_2 dissolution kinetics of $5 \cdot 10^{-3}$M of CO_3^{2-} is stronger than the reduction caused by calcium.

The results obtained by silicate and calcium are consistent with the bibliography. Experimentation with carbonate should be repeated in further experiments, since it is in contradiction with the previous literature and studies.

4.3. Combined influences

Once the effect of the studied compounds has been determined separately, it is proposed to analyse several combinations of compounds and concentrations.

The first case to analyse in Figure 4.8 is the influence of a test solution with **Ca^{2+}** and **SiO_3^{2-}** concentrations of $9.15 \cdot 10^{-4}$ and 10^{-3} M respectively.

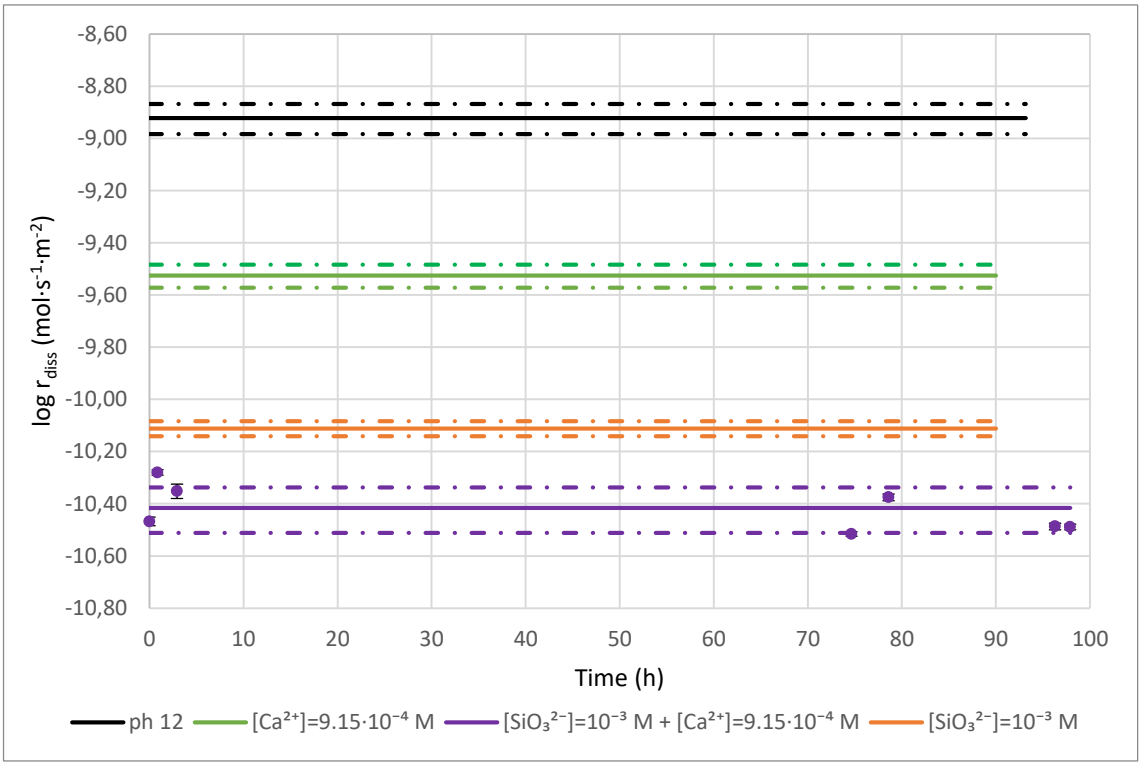

Figure 4.8 Comparison of the dissolution rate logarithm obtained testing an input solution of 10^{-3} M of SiO_3^{2-}. and $9.15 \cdot 10^{-4}$ M of Ca^{2+}.

The kinetics have decreased in presence silicate and calcium, giving a dissolution rate of:

$$pH = 12; [SiO_3^{2-}] = 10^{-3}M; [Ca^{2+}] = 9.15 \cdot 10^{-4}M \rightarrow r_{diss} = (3.84 \pm 0.82) \cdot 10^{-11} \frac{mol}{s \cdot m^2}$$

In comparison with the UO_2 dissolution rate with any other compound, the presence of both silicate and calcium at very low concentration have decreased it by a factor of nearly 40. These results are consistent with the ones obtained by Wilson and Gray (1990). In similar conditions, Espriu-Gascon (2017) performed corrosion studies onto a SIMFUEL electrode, and it was observed that after the electrochemical study, the resulting electrode surface was mainly U(IV). Their results concluded that the cement waters might reduce the corrosion of SNF. The obtained results in this experiment might conclude that cement waters reduce UO_2 dissolution.

The following case analysed is that of $9.15 \cdot 10^{-4}$ M of **Ca^{2+}** with the presence of $2.5 \cdot 10^{-3}$ M of **CO_3^{2-}** (Figure 4.9)

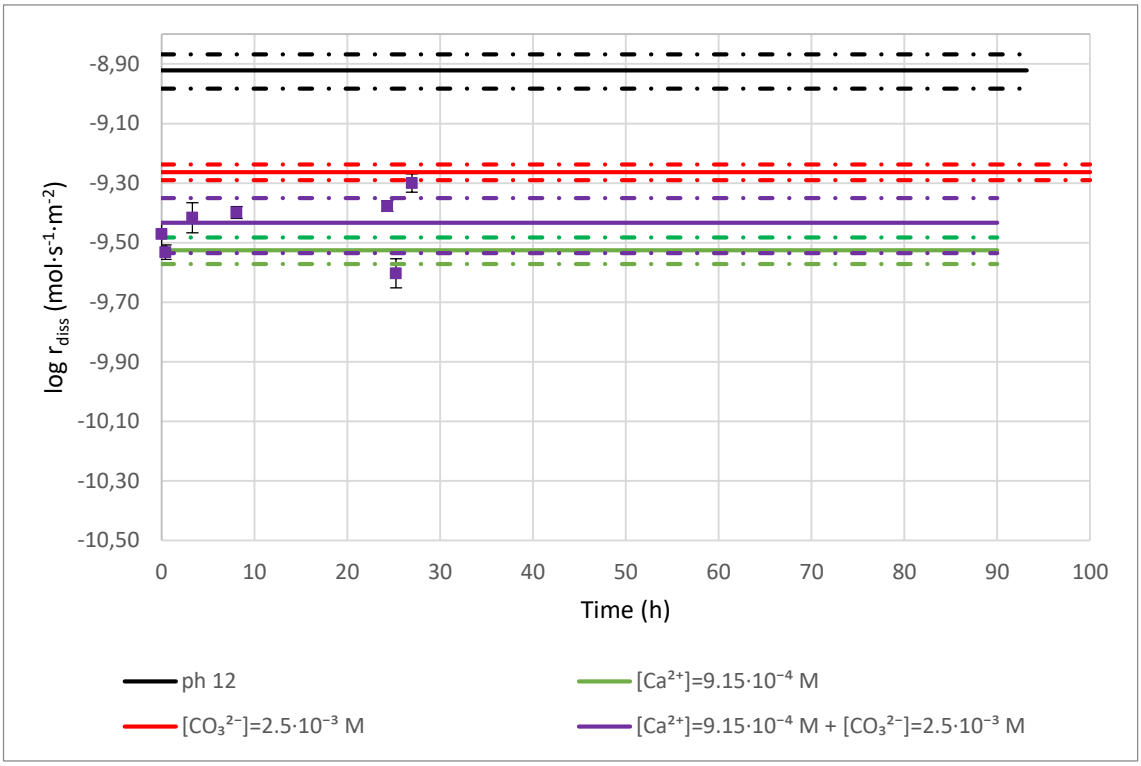

Figure 4.9. Comparison of the dissolution rate logarithm obtained testing an input solution of $9.15 \cdot 10^{-4}$ M of Ca^{2+} and $2.5 \cdot 10^{-3}$ M of CO_3^{2-}.

The obtained dissolution rate is:

$$pH = 12; [Ca^{2+}] = 9.15 \cdot 10^{-4} M; [CO_3^{2-}] = 2.5 \cdot 10^{-3} M \rightarrow r_{diss} = (3.69 \pm 0.84) \cdot 10^{-10} \frac{mol}{s \cdot m^2}$$

As it can be seen, taking into account the huge dispersion of the samples, it is difficult to draw conclusions. It seems that the values approach the dissolution rate given by $2.5 \cdot 10^{-3}$ M of carbonate. But, due to uncertainty it could be concluded that the addition of $2.5 \cdot 10^{-3}$ M carbonate on a calcium solution does not produce a significant variation on the dissolution rate.

Figure 4.10 shows the effect of $5 \cdot 10^{-3}$ M of CO_3^{2-} and SiO_3^{2-} concentrations of 10^{-3}, 10^{-2} and 10^{-1}.

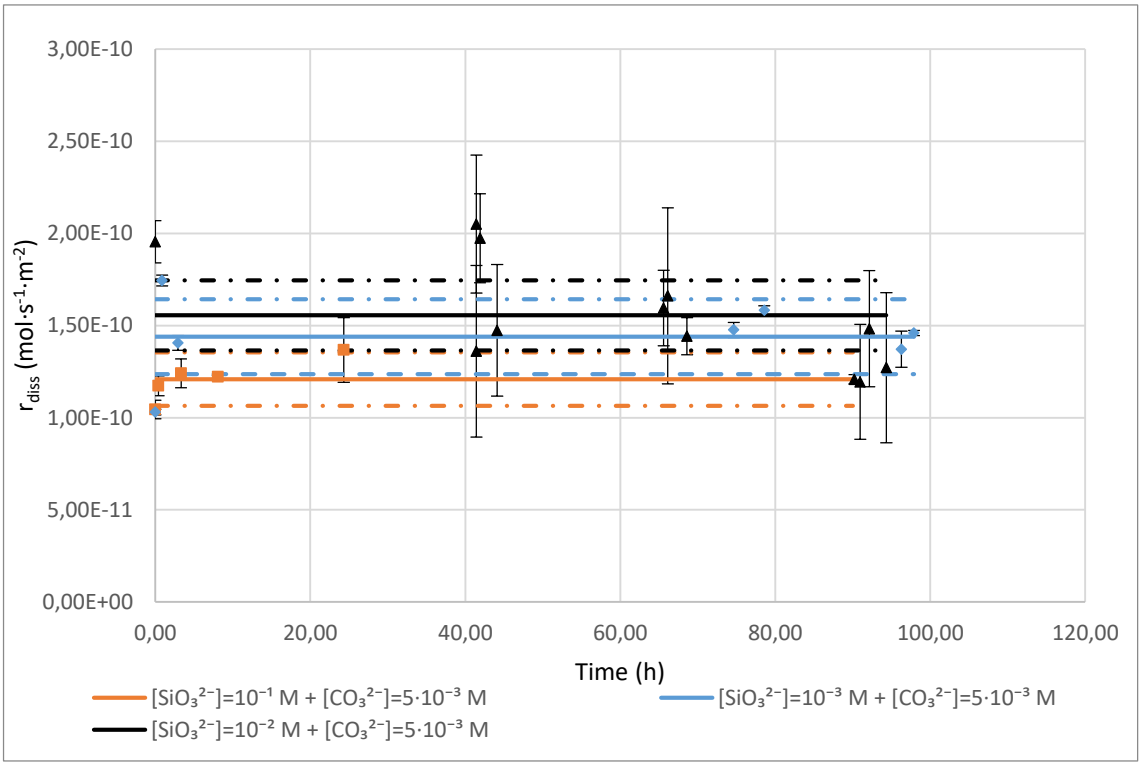

Figure 4.10. Comparison of the dissolution rate obtained testing input solutions of 10^{-3}, 10^{-2} and 10^{-1} M of SiO_3^{2-} with $5\cdot10^{-3}$ M of CO_3^{2-}.

The data overlap dissolution rates around $1\cdot10^{-10}$ and $2\cdot10^{-10}$ mol·s^{-1}·m^{-2}. The obtained kinetics are:

$$pH = 12; [SiO_3^{2-}] = 10^{-3}M; [CO_3^{2-}] = 5 \cdot 10^{-3}M; \rightarrow r_{diss} = (1.44 \pm 0.20) \cdot 10^{-11} \frac{mol}{s \cdot m^2}$$

$$pH = 12; [SiO_3^{2-}] = 10^{-2}M; [CO_3^{2-}] = 5 \cdot 10^{-3}M; \rightarrow r_{diss} = (1.56 \pm 0.19) \cdot 10^{-11} \frac{mol}{s \cdot m^2}$$

$$pH = 12; [SiO_3^{2-}] = 10^{-1}M; [CO_3^{2-}] = 5 \cdot 10^{-3}M; \rightarrow r_{diss} = (1.22 \pm 0.12) \cdot 10^{-11} \frac{mol}{s \cdot m^2}$$

Seeing that the resulting kinetics are ranging the same values, it can be concluded that the SiO_3^{2-} concentration has no influence on the UO_2 dissolution rate when there is CO_3^{2-} in the solution.

The obtained values are compared in Figure 4.11. In this case, due to the data is overlapping, only the experimental results (without confident interval) have been represented to facilitate comparison.

As shown in the figure, the kinetics is faster in the presence of SiO_3^{2-} and CO_3^{2} than when there is only silicate. The obtained dissolution rates for this test are very similar to those of the same concentration of carbonate. Hence, these results suggest that the presence of carbonate may supress the effect of silicate.

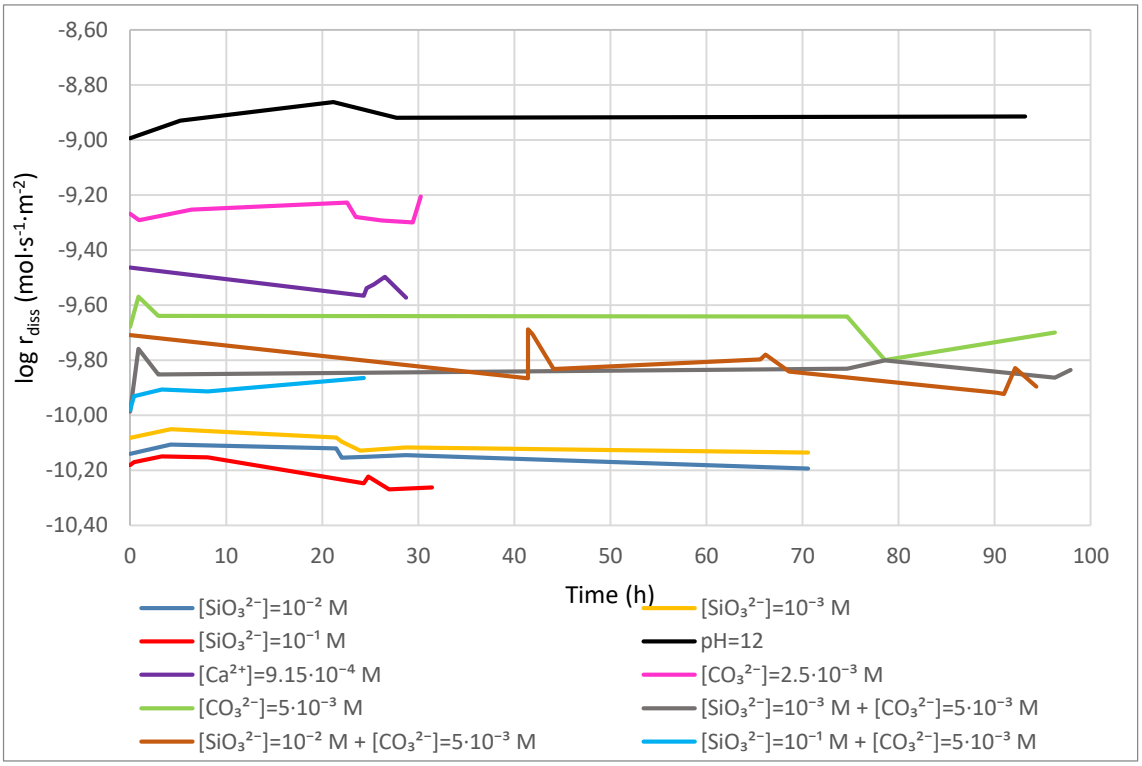

Figure 4.11. Comparison of the dissolution rate logarithm obtained testing input solutions of 10^{-3}, 10^{-2} and 10^{-1} M of SiO_3^{2-} with $5 \cdot 10^{-3}$ M of CO_3^{2-}.

Finally, in the Figure 4.12 are presented and compared the obtained values when the test solution contains **silicate**, **calcium** and **carbonate**.

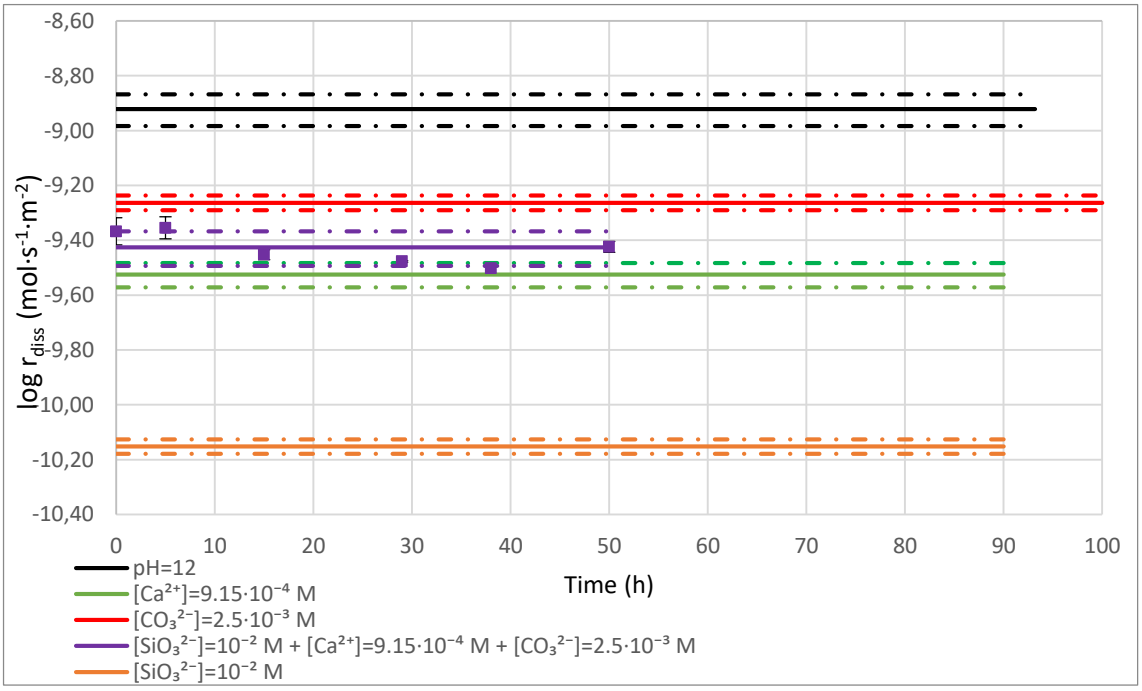

Figure 4.12. Comparison of the dissolution rate logarithm obtained testing an input solution of 10^{-2} M of SiO_3^{2-}, $9.15 \cdot 10^{-4}$ M of Ca^{2+} and $2.5 \cdot 10^{-3}$ M of CO_3^{2-}.

The obtained dissolution rate is:

$$pH = 12; [SiO_3^{2-}] = 10^{-3}M; [Ca^{2+}] = 9.15 \cdot 10^{-4}M; [CO_3^{2-}] = 2.5 \cdot 10^{-3}M; \rightarrow$$

$$r_{diss} = (3.75 \pm 0.54) \cdot 10^{-10} \frac{mol}{s \cdot m^2}$$

In this case, the dissolution rate is accelerated in reference to silicate and calcium, giving very similar values to those when there is only the same concentration of calcium. These results added to the observed by the cases of silicate and carbonate suggest that carbonate might supress the effect of silicate.

The obtained dissolution rates are summarized in Table 4.1.

Table 4.1. Summary of the obtained dissolution rates for each experimented condition.

Test solution	**pH**	**[Na_2SiO_3] (mol·dm^{-3})**	**[$CaCl_2$] (mol·dm^{-3})**	**[Na_2CO_3] (mol·dm^{-3})**	**r_{diss} (mol·s^{-1}·m^{-2})**
OH^-	12	---	---	---	$(1.20 \pm 0.16) \cdot 10^{-9}$
SiO_3^{2-}	12	10^{-3}	---	---	$(7.74 \pm 0.52) \cdot 10^{-11}$
SiO_3^{2-}	12	10^{-2}	---	---	$(7.04 \pm 0.42) \cdot 10^{-11}$
SiO_3^{2-}	12	10^{-1}	---	---	$(5.63 \pm 0.59) \cdot 10^{-11}$
Ca^{2+}	12	---	$9.15 \cdot 10^{-4}$	---	$(2.98 \pm 0.30) \cdot 10^{-10}$
CO_3^{2-}	12	---	---	$2.5 \cdot 10^{-3}$	$(5.46 \pm 0.52) \cdot 10^{-10}$
CO_3^{2-}	12	---	---	$5 \cdot 10^{-3}$	$(2.16 \pm 0.37) \cdot 10^{-10}$
SiO_3^{2-}- Ca^{2+}	12	10^{-3}	$9.15 \cdot 10^{-4}$	---	$(3.84 \pm 0.82) \cdot 10^{-11}$
SiO_3^{2-}- CO_3^{2}	12	10^{-3}	---	$5 \cdot 10^{-3}$	$(1.44 \pm 0.20) \cdot 10^{-10}$
SiO_3^{2-}- CO_3^{2}	12	10^{-2}	---	$5 \cdot 10^{-3}$	$(1.56 \pm 0.19) \cdot 10^{-10}$
SiO_3^{2-}- CO_3^{2}	12	10^{-1}	---	$5 \cdot 10^{-3}$	$(1.22 \pm 0.12) \cdot 10^{-10}$
Ca^{2+}- CO_3^{2}	12	---	$9.15 \cdot 10^{-4}$	$2.5 \cdot 10^{-3}$	$(3.69 \pm 0.84) \cdot 10^{-10}$
Ca^{2+} - SiO_3^{2-}- CO_3^{2}	12	10^{-2}	$9.15 \cdot 10^{-4}$	$2.5 \cdot 10^{-3}$	$(3.75 \pm 0.54) \cdot 10^{-10}$

Once all the cases have been studied, some general conclusions can be drawn.

- Silicate decreases the dissolution rate and has a greater effect than calcium. In the case of SiO_3^{2-}, the higher the concentration, the lower the dissolution rate.
- Calcium and silicates together have an increased effect, decreasing the dissolution kinetics by almost fifty times.
- Contrary to what it was expected, in this the study results show that the presence of carbonate decreases the dissolution rate.
- It can be concluded that carbonate may inhibit the effects of silicate. In all the silicate solutions where carbonate is present, the value of the UO_2 dissolution rate is increased respect to those with the same concentration of only silicate.

4.4. Characterization

In order to obtain a chemical analogue of Gd-doped SNF, the synthesized pellets must have similar properties to commercial doped fuels. To observe if the sintered pellets met the requirements, a characterization process was performed with the adequate techniques.

The pellet specification requires that at least 94% of the added gadolinia forms solid solution with uranium. The remaining 6% may exist as free (unreacted) Gd_2O_3 particles larger than 20 µm. Of these, 2% may exist as particles in the range 40-100 µm (Hälldahl and Eriksson, 1988).

4.4.1. SEM Results

Several SEM scans were performed before and after the synthetisation.

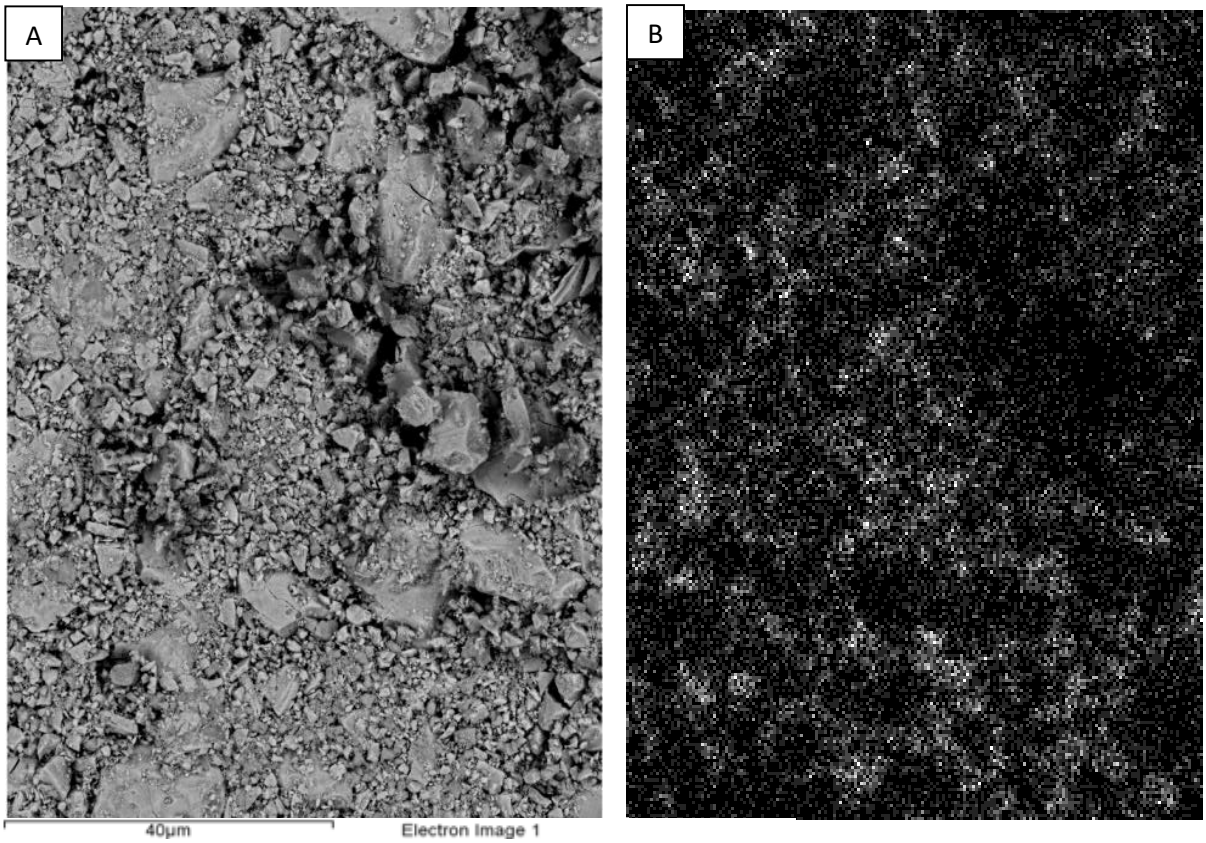

Figure 4.13. A. Gd-doped pellet analysed by SEM prior to the synthetization. B. Elemental mapping of gadolinium (white) and uranium (black).

Scanning previous to sintering aimed to observe if gadolinium had a good dispersion into the UO_2 matrix. From the atomic weight difference, SEM distinguished gadolinium oxide from uranium oxide As shown in Figure 4.13, qualitatively, there is a homogeneous dispersion into the pellet.

Furthermore, from that scan, it was observed that the particle size ranged from a few micrometres to few tens of micrometres. The particle diameter was adjusted to 10-20 µm for the subsequent experiments.

After the synthesis, the pellet changed its aspect. New phases were formed and grains of distinct compositions and grain boundaries can be distinguished. These changes can be seen in Figure 4.14 and Figure 4.15.

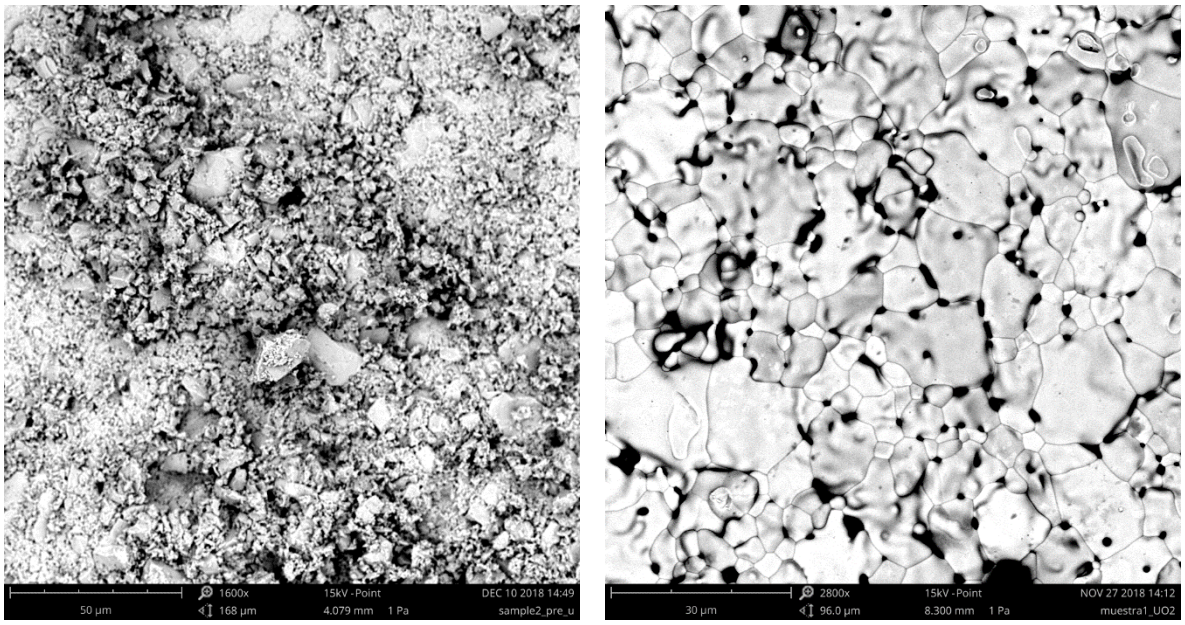

Figure 4.14. SEM images of UO_2 samples prior (left) and after (right) to the sintering.

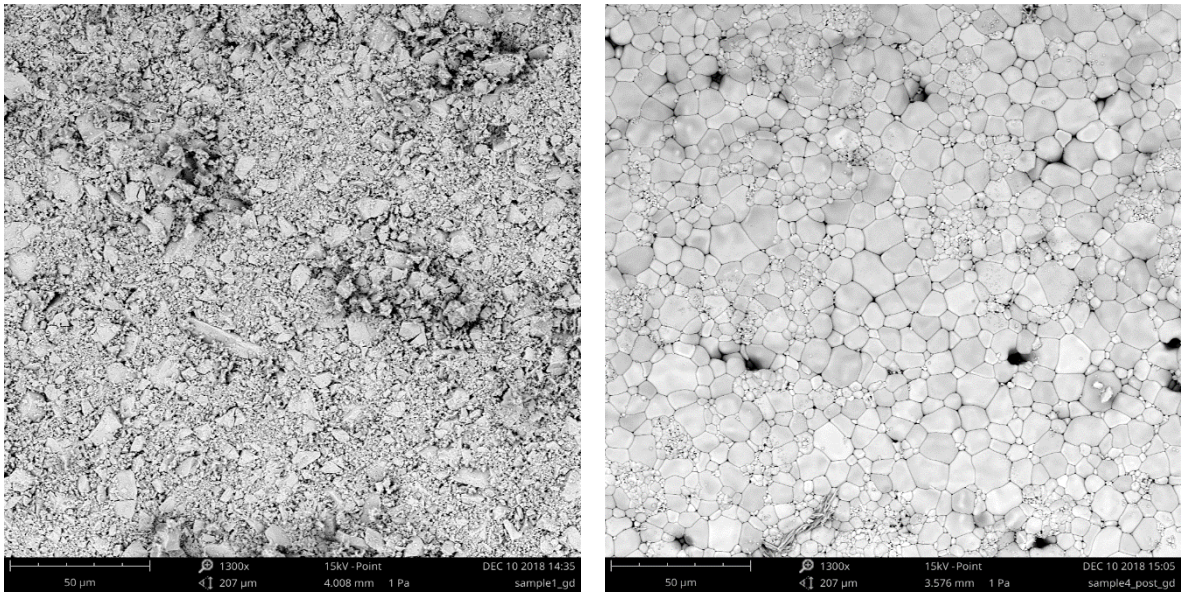

Figure 4.15. SEM images of Gd-doped samples prior (left) and after (right) to the sintering.

Elemental analysis by Energy Dispersive Spectrometry (EDS) was performed to analyse the homogeneity of the samples. Results are shown in Figure 4.16. for the pure UO_2 pellets, and in Figure 4.17 for the Gd-doped pellets.

Referring to the undoped sample, it was found what it was expected: the uranium had melted, resulting in new pure phases of uranium, shown in points 1 and 3. Although due to the fact that the crucible reacted with the pellet during the sintering process, there is presence of aluminium phases in it, which can be identified as the black zones (point 3).

For the Gd-doped samples, in the locations 1,2 and 4, Gd and UO_2 formed a new phase of both solids with the desired concentration of Gd. Instead, in point 5, there is an enriched zone of Gd. Considering the fabrication method, a complete homogeneous distribution of gadolinium throughout the samples is impossible to achieve. Very small particles with high gadolinium content were indeed observed. At zones with a lighter coloration, a higher density of pores was often observed. The different shades may indicate concentration variations, with higher content of Gd in the darker zones and lower Gd content in the lighter zones. Meanwhile in 3, some incongruences appeared, this is due to the fact that during the sintering, the pellet reacted with the melting pot.

Furthermore, it was observed for both pellets that, despite sieving to a range of 10-20 µm in certain areas there were many grouped particles of smaller size than 10 µm, which does not meet the requirements for nuclear fuel pellets. Consequently, several parts of the process must be improved.

- Despite using sieves of 10 and 20 µm, it seems that the smaller particles are grouped with the larger ones, making the sieving process difficult. Consequently, this process will have to be improved using for example a sieving shaker or ultrasounds.
- Alumina crucibles reacted with the samples. It is necessary to find another substitute for these crucibles, such as molybdenum.

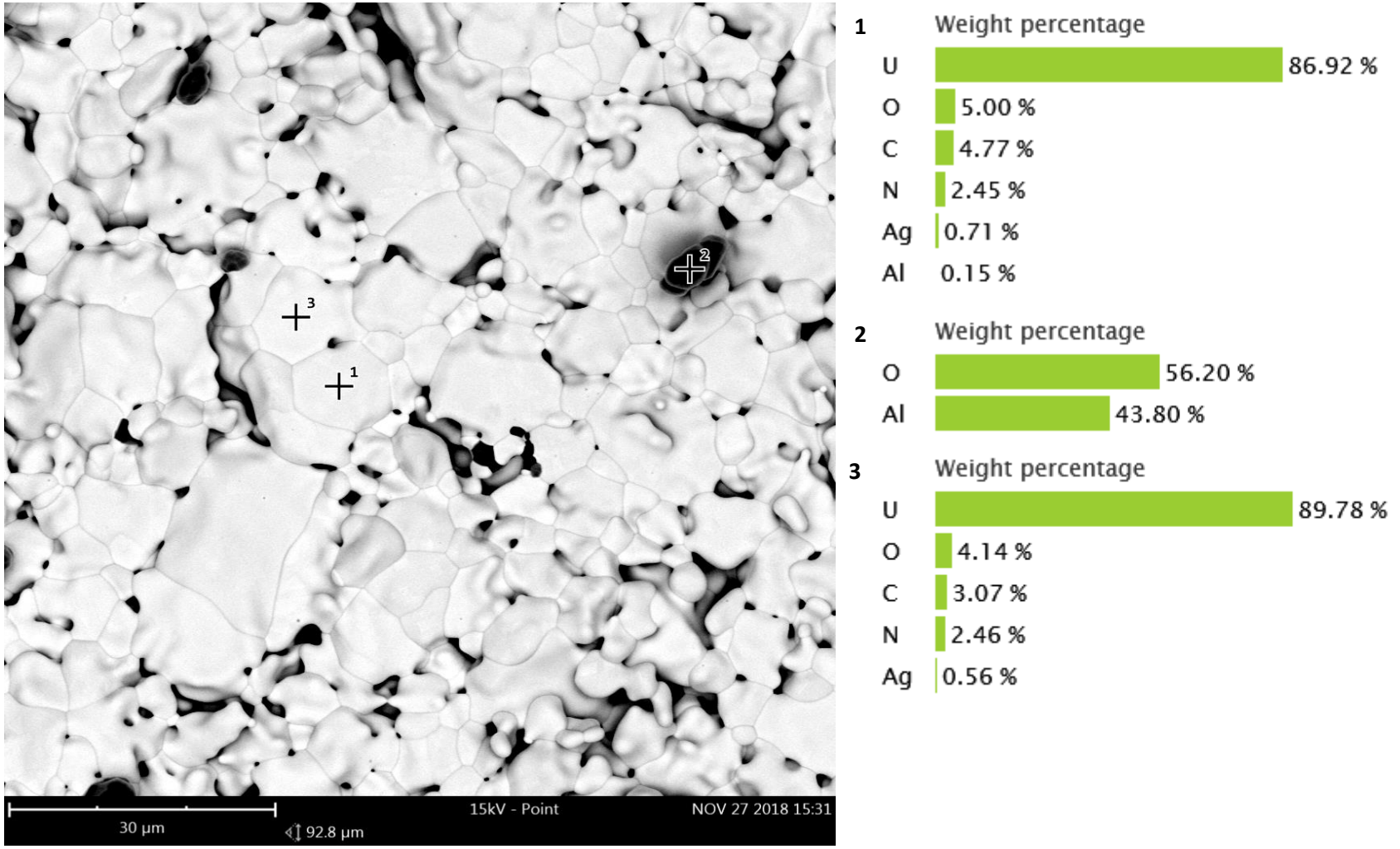

Figure 4.16. Image obtained by SEM and EDS study performed to the pure UO2 pellet.

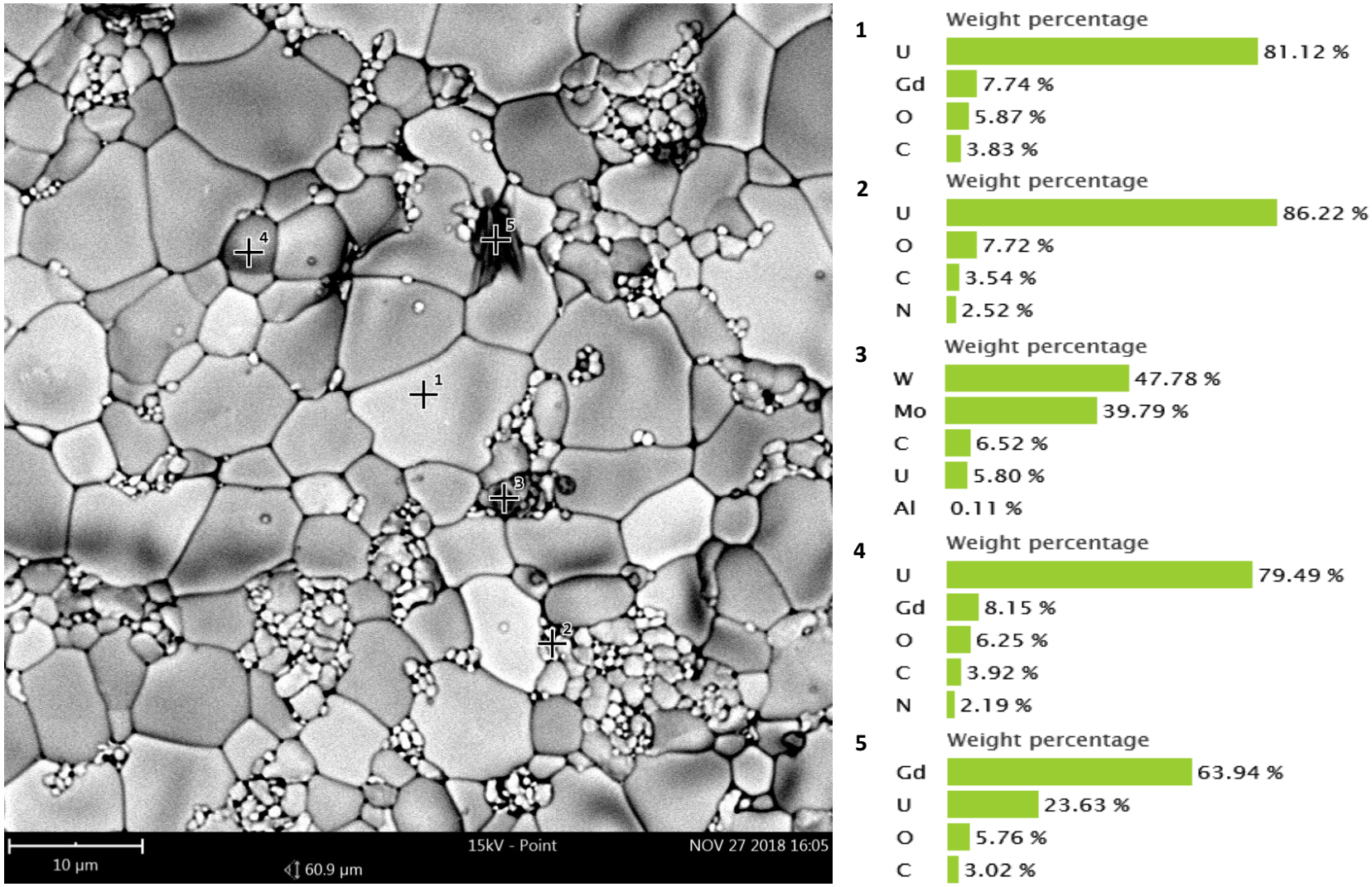

Figure 4.17. Image obtained by SEM and EDS study performed on the Gd-doped pellet.

4.4.2. XRD Results

XRD can be used to quantitatively determine the quality of the sintered Gd-pellet. It allows the determination of the phases that have been formed. Moreover, some methods permit to calculate the amount of unreacted Gd that may exist in the system.

Unfortunately, in this work it has not been possible to achieve a good analysis due to the small amount of sample produced was not enough for XRD. This has resulted in diffractograms with a lot of noise from which quantitative information cannot be extracted. Due to the impossibility to extract good conclusions, the results obtained by other investigations will be discussed before showing the diffractograms.

X-ray diffraction analysis would have shown the presence of only one crystalline phase (fluorite type). As a result of new phases formed during the sintering, the position of the peaks on the X-Ray diffractogram is displaced (Figure 4.18). This displacement is related with the lattice parameter, which decreases with increase in concentration of Gd (Kapoor *et al.*, 2003).

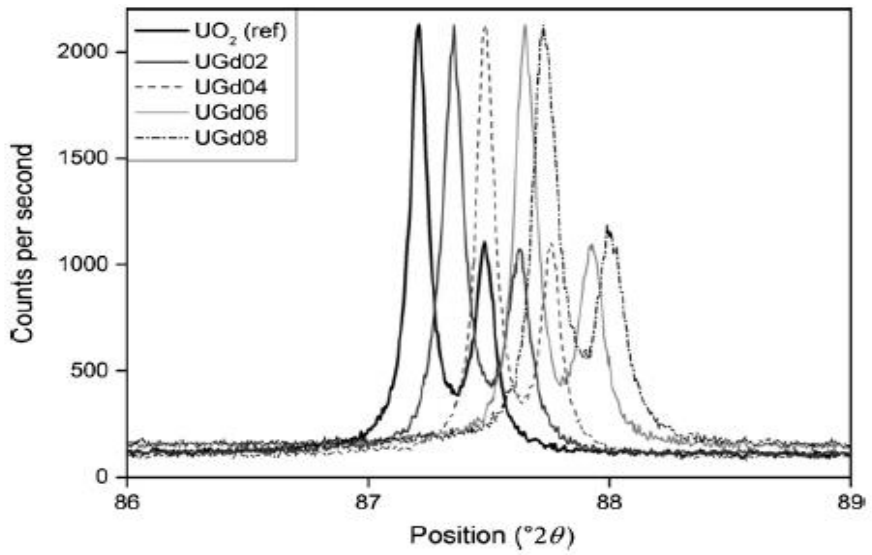

Figure 4.18. X-ray analysis performed by Baena et al. (2015). It is shown the displacement of the peaks for different Gd concentrations.

Another study that would be interesting to apply to the obtained X-ray powder diffraction data is the Rietveld method. The shape of the peaks changes asymmetrically when phases of similar cell parameter coexist. The Rietveld method allows to evaluate this asymmetry simulating the pattern with a model of two phases each with its own cell parameters. With the adequate parameters, the value of the lattice parameter can be used to quantify the Gd amount that constitute the solid solution (Leyva *et al*. 2002).

In the obtained diffractograms (Figure 4.19 and Figure 4.20) the characteristics peaks of UO_2 and Gd_2O_3 are distinguished. Due to the noise, the displacement of the peaks cannot be seen.

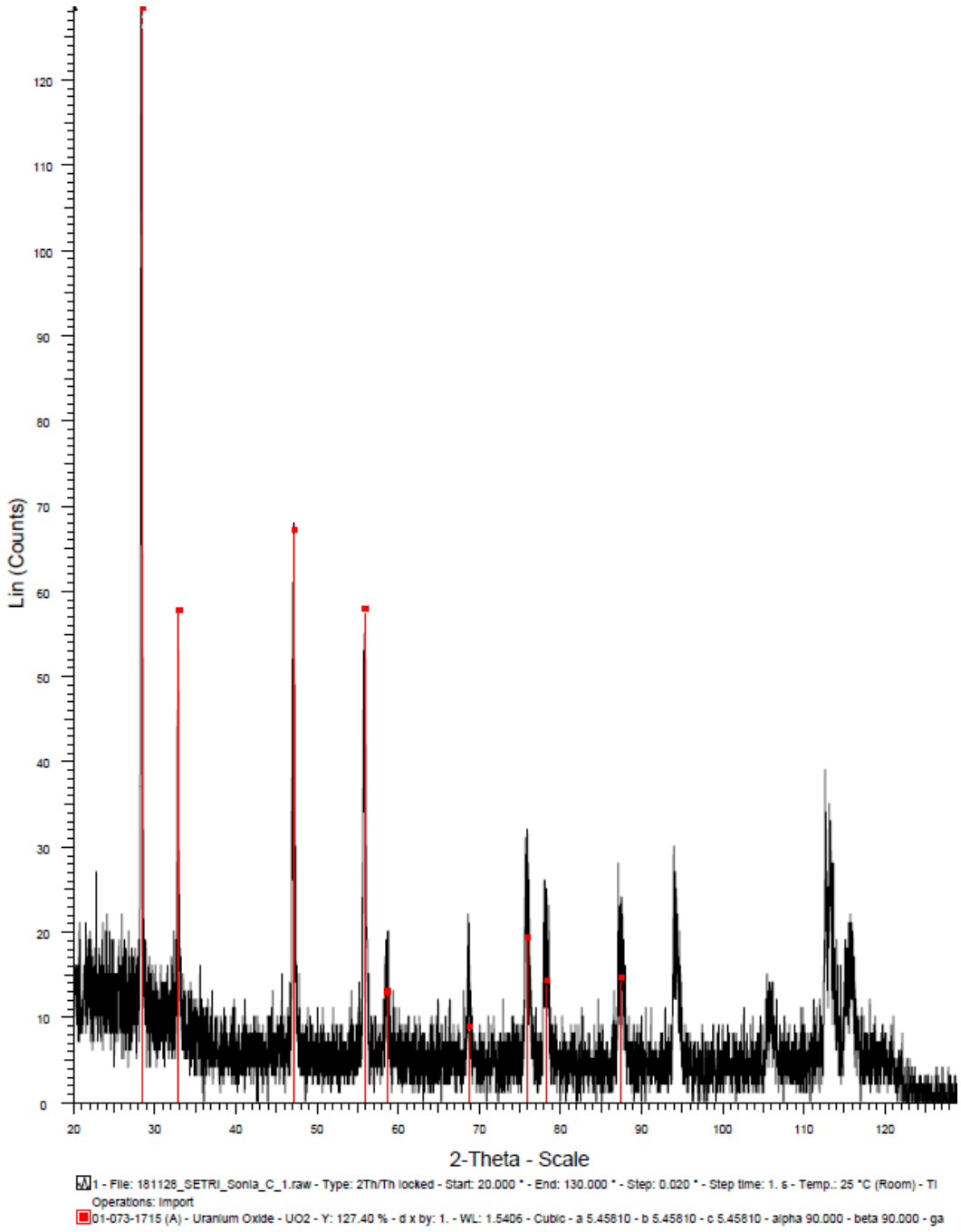

Figure 4.19. UO_2 pellet XRD spectrum and characteristic peaks for UO_2 from EVA database.

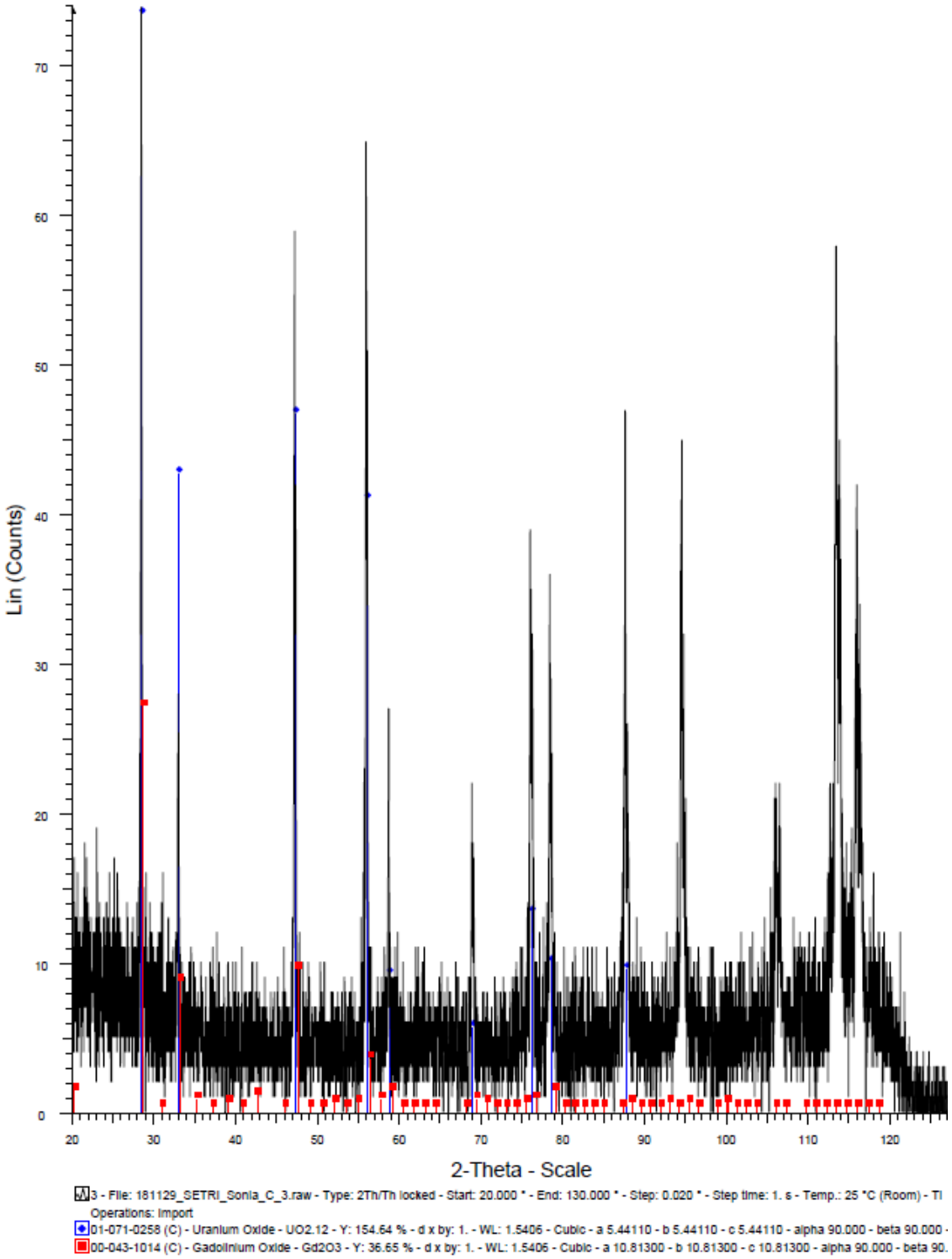

Figure 4.20. Gd-doped pellet XRD spectrum and characteristic peaks for UO2 (red) and Gd2O3 (blue) from EVA database.

5. Conclusions

In this section the conclusions of the experimental work are presented.

The following conclusions can be extracted from the performed kinetic study:

- As intended, a system with several thin layer reactors has been put into operation.
- It has been possible determine the UO_2 dissolution rate in each tested condition.
- Certain trends have been identified from the kinetic studies of calcium, silicate and carbonate in alkaline conditions:
    - The UO_2 dissolution rate at hyper alkaline conditions (pH=12) is higher than at neutral pH.
    - The presence of Ca^{2+} and SiO_3^{2-} decreases the dissolution rate.
    - The inhibitory effects of silicate are higher than that of calcium. The higher the SiO_3^{2-} concentration, the slower the UO_2 kinetics.
    - In this study, the presence of CO_3^{2-} decreases the dissolution rate. Further investigations have to be performed in this regard.
    - Both calcium and silicate together in dissolution give the greatest inhibitory force. When using concentrations of 10^{-3} and $9.15 \cdot 10^{-4}$ M of silicate and calcium, respectively, the UO_2 dissolution rate is almost 50 times slower.
    - The presence of carbonate may block the effects caused by silicate.
- From the results of this work, it can be concluded that the cement waters might reduce SNF dissolution.
- The effect of carbonate from groundwater combined with cement water on the UO_2 kinetics needs to be studied further in future investigations.

Regarding the manufacture and characterization of Gd-doped pellets:

- Despite all the difficulties encountered during the manufacturing process, the sintering and characterization process have performed.
- By SEM, it has been observed that the pellet has taken the desired appearance. Some parts of the synthesis process, though, must be improved:
    - It is necessary to have a different crucible: it should not react with the pellet at the high temperatures needed in the sintering process.
    - The sieving process must be improved, since small particles adhere to the bigger ones, thus becoming part of the pellet.
- More sample will be required in order to perform the XRD scan correctly, no information could be extracted from the obtained diffractograms.

6. Waste management

The used material that might contain remnants of UO_2 powder is cleaned with a nitric acid 2 wt% dissolution. Nitric acid oxidises U(IV) to U(VI), making the cleaning process easier by increasing its solubility in water.

Two kinds of waste in need of different treatments are generated in this project:

On one hand, adsorbent solids that have been in contact with uranium, as gloves, paper, filters, etc. These materials are disposed in bags. Once they are full, they are weighted and the emitted radiation is measured; if it is lower than 50 mSv, which is the maximum dose received established by official organisms (Consejo de Seguridad Nuclear, 2010), this waste can be categorised as a normal waste. If the concentration exceeded said amount, the waste will need to be regarded as radioactive, thus requiring a much more complex and meticulous treatment.

On the other hand, dissolutions containing uranium, which come from the cleaning process and the reactors, are disposed in 20 L drums. The drum will be classified as an aqueous acid inorganic solution containing heavy metals (Figure 6.1). Finally, a sample will be taken. If the total uranium concentration is lower than 3 ppm, the solution can be treated as a normal waste.

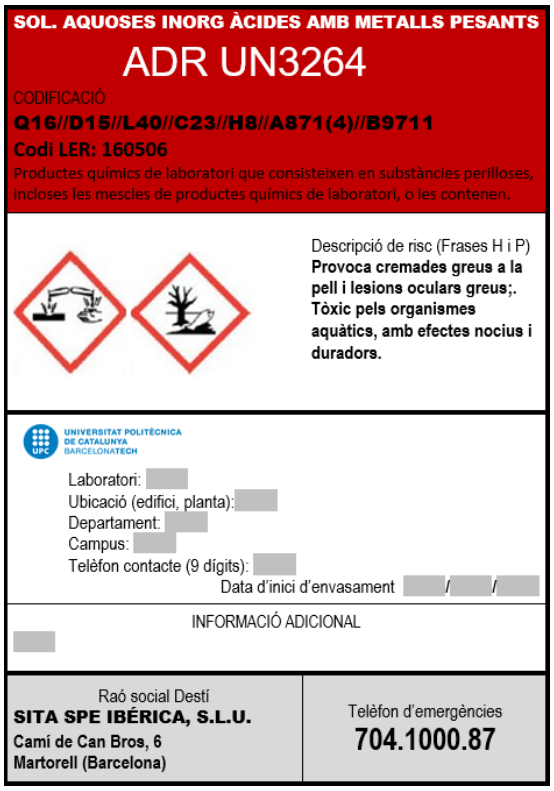

Figure 6.1. Waste classification for aqueous dissolution containing dissolved uranium.

7. Economic study

The total expense during the performance of this project is detailed in this section. It is detailed in terms of equipment, laboratory supply, reagents and human resources

The cost related to equipment is calculated as amortization cost in function of its acquisition cost, service time and using time during the project (Table 7.1). It is considered that the amortization cost is homogeneous over time.

$$Amortization = \frac{Acquisition\ cost}{service\ time} \cdot using\ time \quad (21)$$

Table 7.1. Amortization calculation cost

Equipment	Acquisition cost (€)	Service time (years)	Using time (years)	Amortization (€)
Horizontal Furnace	22000.00	10	0.5	1100.00 €
Peristaltic pump	1609.20	10	0.5	80.46 €
Manual press	2860.00	15	0.5	95.33 €

It is supposed a cost of 300 € for that equipment used during the experiments which have been reused from other projects, such as volumetric flasks, spatulas, the agar mortar, pipettes, tubing for peristaltic pumps, etc.

Table 7.2. Total costs of the project.

PROJECT COSTS					
	Description	**Unit price**	**Unit**	**Number**	**Total price**
1. HUMAN RESOURCES					
1.1.	**Experimentation.** Planning and realization of experimental work	12.00 €	h	250.00	3,000.00 €
1.2.	**Elaboration of the report** Writing and bibliographical research.	12.00 €	h	280.00	3,360.00 €
	SUBTOTAL				**6,360.00 €**
2. EQUIPMENT					
2.1.	**Horizontal tube furnace** Hobersal ST196030 HG	1100.00 €	u	1.00	1,100.00 €
2.2.	**Manual hydraulic press** Specac Atlas 15t manual hydraulic press	95.33 €	u	1.00	95.33 €
2.3.	**Peristaltic pump** Heidolph® Pumpdrive PD 5001	80.46 €	u	2.00	160.92 €
2.4.	**Miscellaneous** Glass material, pipettes, tubing, etc.	300.00 €	u	1.00	300.00 €

	SUBTOTAL				**1,656.25 €**
3. REAGENTS AND LABORATORY SUPPLY					
3.1.	**Sodium hydroxide 1 M** Pure quality for analysis	33.90 €	L	1.00	33.90 €
3.3.	**Nitric acid 90%.** Pure quality for analysis	39.50 €	L	0.10	3.95 €
3.3.	**Sodium carbonate** Pure quality for analysis	43.60 €	kg	0.05	3.13 €
3.4.	**Sodium silicate** General purpose grade	49.50 €	kg	0.10	4.95 €
3.4.	**Calcium chloride 3-hydrate** Pure quality for analysis	30.00 €	kg	0.05	1.50 €
3.5.	**Gadolinium (III) oxide** Pure quality for analysis	3120.00 €	kg	0.001	3.12 €
3.6.	**Nitrogen bottle**	55.53 €	kg	1.00	55.53 €
3.7.	**Argon and hydrogen bottle**	83.66 €	u	1.00	83.66 €
3.8.	**10 mL plastic test tubes and plug**	0.08 €	u	355.00	18.45 €
3.9.	**Plug for 10 mL plastic test tubes**	0.05 €	u	335.00	11.35 €
3.10.	**1 mL pipette tips**	0.05 €	u	350.00	13.60 €
3.11.	**5 mL pipette tips**	0.11 €	u	50.00	50.35 €
3.12.	**Gloves** Nitrile gloves free powder	0.06 €	u	100.00	6.20 €
3.13.	**Parafilm.** Parafilm 10 x 38 cm	0.63 €	m	5.00	3.15 €
3.14.	**Millipore filters 0.22 µm** Diameter 13 mm	0.03 €	u	30.00	0.90 €
3.15.	**Filterholder** From Swinnex®, internal diameter 13 mm	4.80	u	6.00	28.80
	SUBTOTAL				**322.84**
3. ENERGY					
4.1.	**Electric energy**	0.137 €	kWh	302.40	41.42 €
	SUBTOTAL				**41.42 €**
	GROSS TOTAL COST				**8,380.51 €**
	V.A.T. (21%)				**1,759.91 €**
	NET TOTAL COST				**10,140.42 €**

Bibliography

Aceto, M. (2016) 'The Use of ICP-MS in Food Traceability', *Advances in Food Traceability Techniques and Technologies*. Elsevier Ltd, pp. 137–164. doi: 10.1016/B978-0-08-100310-7.00008-9.

Andra (2018) *Cigéo Project: Deep geological disposal facility for radioacive waste in Meuse/Haute-Marne departments*.

Arborelius, J., Backman, K., Hallstadius, L., Limbäck, M., Nilsson, J., Rebensdorff, B., Zhou, G., Kitano, K., Löfström, R. and Rönnberg, G. (2006) 'Advanced doped UO2pellets in LWR applications', *Journal of Nuclear Science and Technology*, 43(9), pp. 967–976. doi: 10.1080/18811248.2006.9711184.

Azkárate, I., Madina, V. and Insausti, M. (1999) *Estudios de corrosión de materiales metalicos para capsulas de almacenamiento de residuos de alta actividad*.

Baena, A., Cardinaels, T., Vos, B., Binnemans, K. and Verwerft, M. (2015) 'Synthesis of UO2and ThO2doped with Gd2O3', *Journal of Nuclear Materials*, 461, pp. 271–281. doi: 10.1016/j.jnucmat.2015.03.028.

Birkholz, M. (2006) 'Principles of X-ray diffraction', in *Thin Film Analysis by X-Ray Scattering*. Wiley-VCH Verlag GmbH & Co. KGaA, pp. 1–41. doi: 10.1002/3527607595.ch1.

Bruno, J., Casas, I. and Puigdomènech, I. (1991) 'The kinetics of dissolution of UO2under reducing conditions and the influence of an oxidized surface layer (UO2+x): Application of a continuous flow-through reactor', *Geochimica et Cosmochimica Acta*, 55(3), pp. 647–658. doi: 10.1016/0016-7037(91)90330-8.

Bruno, J. and Ewing, R. C. (2006) 'Spent Nuclear Fuel', pp. 343–350.

Burnable Absorbers (no date). Available at: https://www.nuclear-power.net/nuclear-power-plant/nuclear-fuel/burnable-absorbers-burnable-poisons/ (Accessed: 13 November 2018).

Casas, I. (1989) *Estudios físico-químicos de la disolución del UO2*. Universitat Politècnica de Catalunya (UPC).

Casas, I., Gimenez, J., Marti, V., Torrero, M. E. and de Pablo, J. (1994) 'Kinetic studies of unirradiated UO2 dissolution under oxidizing conditions in batch and flow experiments', *Radiochimica Acta*, 66/67, pp. 23–27. doi: 10.1524/ract.1994.6667.special-issue.23.

Consejo de Seguridad Nuclear (2010) *Dosis de Radiación*. Madrid.

ENRESA (2014) *7o Plan Nacional De I + D. 2014-2018.* Madrid.

Espriu-Gascon, A. (2017) *Study of near field processes involved in the oxidative dissolution of the spent nuclear fuel and radionuclides release*. Universitat Politècnica de Catalunya (UPC).

Espriu-Gascon, A., Shoesmith, D. W., Giménez, J., Casas, I. and De Pablo, J. (2017) 'Study of SIMFUEL corrosion under hyper-alkaline conditions in the presence of silicate and calcium', *MRS Advances*,

2(10), pp. 543–548. doi: 10.1557/adv.2016.619.

Ewing, R. C. (2015) 'Long-term storage of spent nuclear fuel', *Nature Materials*. Nature Publishing Group, 14(3), pp. 252–257. doi: 10.1038/nmat4226.

Fuel Burnup (no date). Available at: https://www.nuclear-power.net/nuclear-power/reactor-physics/reactor-operation/fuel-burnup/ (Accessed: 30 November 2018).

Giménez, J., Clarens, F., Casas, I., Rovira, M., De Pablo, J. and Bruno, J. (2005) 'Oxidation and dissolution of UO2in bicarbonate media: Implications for the spent nuclear fuel oxidative dissolution mechanism', *Journal of Nuclear Materials*, 345(2–3), pp. 232–238. doi: 10.1016/j.jnucmat.2005.06.003.

Hälldahl, L. and Eriksson, S. (1988) 'Characterization of homogeneity in (U, Gd)O2-pellets', *Journal of Nuclear Materials*, 153(C), pp. 66–70. doi: 10.1016/0022-3115(88)90193-6.

IAEA (1995) 'Characteristics and Use of Urania-Gadolinia Fuels', pp. 1–191. doi: IAEA-TECDOC--844.

Kapoor, K., Ramana Rao, S. V., Sheela, Sanyal, T. and Singh, A. (2003) 'Study on solid solubility of Gd in UO2using X-ray diffraction', *Journal of Nuclear Materials*, 321(2–3), pp. 331–334. doi: 10.1016/S0022-3115(03)00239-3.

Kim, J. G., Ha, Y. K., Park, S. D., Jee, K. Y. and Kim, W. H. (2001) 'Effect of a trivalent dopant, Gd3+, on the oxidation of uranium dioxide', *Journal of Nuclear Materials*, 297(3), pp. 327–331. doi: 10.1016/S0022-3115(01)00639-0.

Levenspiel, O. (1999) 'Chemical Reaction Engineering', in Ken, S. (ed.) *Chemical Engineering Engineering*. 3rd edn. New York: John Willey & Sons, p. 369. doi: 10.1016/0009-2509(64)85017-X.

Leyva, A. G., Vega, D., Trimarco, V. and Marchi, D. (2002) 'Homogeneity characterisation of sintered (U,Gd)O2 pellets by X-ray diffraction', *Journal of Nuclear Materials*, 303(1), pp. 29–33. doi: 10.1016/S0022-3115(02)00819-X.

Liu, N., Kim, J., Lee, J., Youn, Y. S., Kim, J. G., Kim, J. Y., Noël, J. J. and Shoesmith, D. W. (2017) 'Influence of Gd Doping on the Structure and Electrochemical Behavior of UO2', *Electrochimica Acta*, 247, pp. 496–504. doi: 10.1016/j.electacta.2017.07.006.

Marinceu, D. and Murchison, A. (2018) 'Automated Buffer Box Assembly Cell Concept for the Canadian Used Fuel Packing Plant', (March).

Massih, A. (2014) 'Effects of additives on uranium dioxide fuel behavior', p. 74. doi: 21ISSN:2000-0456.

Nilsson, K., Roth, O. and Jonsson, M. (2017) 'Oxidative dissolution of ADOPT compared to standard UO2fuel', *Journal of Nuclear Materials*. Elsevier B.V., 488, pp. 123–128. doi: 10.1016/j.jnucmat.2017.02.044.

De Pablo, J., Casas, I., Giménez, J., Clarens, F., Duro, L. and Bruno, J. (2004) 'The oxidative dissolution mechanism of uranium dioxide. The effect of pH and oxygen partial pressure', 807(1), pp. 1–6.

De Pablo, J., Casas, I., Giménez, J., Molera, M., Rovira, M., Duro, L. and Bruno, J. (1999) 'The oxidative dissolution mechanism of uranium dioxide. I. The effect of temperature in hydrogen carbonate

medium', *Geochimica et Cosmochimica Acta*, 63(19–20), pp. 3097–3103. doi: 10.1016/S0016-7037(99)00237-9.

Razdan, M. and Shoesmith, D. W. (2013) 'Influence of Trivalent-Dopants on the Structural and Electrochemical Properties of Uranium Dioxide (UO2)', *Journal of the Electrochemical Society*, 161(3), pp. H105–H113. doi: 10.1149/2.047403jes.

Razdan, M. and Shoesmith, D. W. (2014) 'The Electrochemical Reactivity of 6.0 wt% Gd-Doped UO2 in Aqueous Carbonate/Bicarbonate Solutions', *Journal of the Electrochemical Society*, 161(4), pp. H225–H234. doi: 10.1149/2.050404jes.

Roth, O. and Jonsson, M. (2008) 'Oxidation of UO2(s) in aqueous solution', *Central European Journal of Chemistry*, 6(1), pp. 1–14. doi: 10.2478/s11532-007-0067-z.

Santos, B. G., Noël, J. J. and Shoesmith, D. W. (2006a) 'The effect of pH on the anodic dissolution of SIMFUEL (UO2)', *Electrochimica Acta*, 586, pp. 1–11. doi: 10.1016/j.jelechem.2005.09.021.

Santos, B. G., Noël, J. J. and Shoesmith, D. W. (2006b) 'The influence of calcium ions on the development of acidity in corrosion product deposits on SIMFUEL (UO2)', *Journal of Nuclear Materials*, 350(3), pp. 320–331. doi: https://doi.org/10.1016/j.jnucmat.2006.02.002.

Santos, B. G., Noël, J. J. and Shoesmith, D. W. (2006c) 'The influence of silicate on the development of acidity in corrosion product deposits on SIMFUEL (UO2)', *Corrosion Science*, 48(11), pp. 3852–3868. doi: 10.1016/j.corsci.2006.02.012.

Savage, D. (1995) *The scientific and regulatory basis for the geological disposal of radioactive waste*. 1st edn. Chichester: John Willey & Sons.

Shoesmith, D. W. (2000) 'Fuel corrosion processes under waste disposal conditions', *Journal of Nuclear Materials*, 282(1), pp. 1–31. doi: 10.1016/S0022-3115(00)00392-5.

Skoog, D. A., Holler, F. J. and Crouch, S. R. (2008) *Pricipios de Análisis Instrumental*. 6th edn. México D.F.: Cencage Learning.

Stumm, W. (1992) *Chemistry of the Solid-Sater Interface. Processes at the Mineral-Water and Particle-Water Interface in Natural Systems*. 1st edn, *New York*. 1st edn. John Willey & Sons.

Stumm, W. and Wollast, R. (1990) 'Coordination chemistry of weathering: Kinetics of the surface-controlled dissolution of oxide minerals', *Reviews of Geophysics*, 28(1), pp. 53–69.

Thomas, G. F. and Till, G. (1984) 'The dissolution of unirradiated UO2 fuel pellets under simulated disposal conditions', *Nuclear and Chemical Waste Management*, 5(2), pp. 141–147. doi: 10.1016/0191-815X(84)90044-5.

Torrero, M. E. (1995) *Estudio de la disolución del UO2 como análogo químico de la matriz del combustible nuclear gastado*. Universitat Politècnica de Catalunya (UPC).

Wilson, C. N. and Gray, W. J. (1990) 'Measurement of soluble nuclide dissolution rates from spent fuel', *Scientific for Nuclear Waste Management XIII*, 176, p. 489.

Zhou, W., Apkarian, R., Wang, Z. L. and Joy, D. (2007) 'Fundamentals of scanning electron microscopy (SEM)', *Scanning Microscopy for Nanotechnology: Techniques and Applications*, pp. 1–40. doi: 10.1007/978-0-387-39620-0_1.

Annex A: Experimental data

In this section all the experimented data is presented.

Table 0.1. Obtained values for an input solution at pH=12 without the effect of any compound

Total time (h)	Flow rate (mL/min)	[U] (ppb)	r_{diss} ($mol \cdot s^{-1}$)	r_{diss} ($mol \cdot s^{-1} \cdot m^{-2}$)
0.00	0.20 ± 0.02	452± 11.4	$6.29 \cdot 10^{-12}$	$(3.97 \pm 0.09) \cdot 10^{-9}$
3.52	0.19 ± 0.02	405 ± 9.23	$5.30 \cdot 10^{-12}$	$(3.35 \pm 0.08) \cdot 10^{-9}$
21.47	0.11 ± 0.02	1579 ± 80.5	$1.24 \cdot 10^{-11}$	$(7.81 \pm 0.42) \cdot 10^{-9}$
43.72	0.11 ± 0.02	2401 ± 30.7	$1.84 \cdot 10^{-11}$	$(1.16 \pm 0.17) \cdot 10^{-9}$
46.67	0.11± 0.02	211 ± 5.22	$1.61 \cdot 10^{-12}$	$(1.02 \pm 0.03) \cdot 10^{-9}$
51.92	0.10 ± 0.02	253.1 ± 30.1	$1.86 \cdot 10^{-12}$	$(1.18 \pm 0.12) \cdot 10^{-9}$
67.82	0.17 ± 0.02	211 ± 5.63	$2.54 \cdot 10^{-12}$	$(1.60 \pm 0.04) \cdot 10^{-9}$
74.38	0.11 ± 0.02	304 ± 8.41	$2.41 \cdot 10^{-12}$	$(1.07 \pm 0.50) \cdot 10^{-9}$
139.85	0.07 ± 0.02	414 ± 60 .7	$1.93 \cdot 10^{-12}$	$(1.22 \pm 0.17) \cdot 10^{-9}$

Table 0.2. Obtained data testing an input solution of $9.15 \cdot 10^{-4}$ M of Ca^{2+}.

Total time (h)	Flow rate (mL/min)	[U] (ppb)	r_{diss} ($mol \cdot s^{-1}$)	r_{diss} ($mol \cdot s^{-1} \cdot m^{-2}$)
0.00	0.40 ± 0.02	23.75 ± 3.43	$6.61 \cdot 10^{-13}$	$(3.44 \pm 0.50) \cdot 10^{-10}$
24.32	0.35 ± 0.02	21.56 ± 1.59	$5.23 \cdot 10^{-13}$	$(2.72 \pm 0.20) \cdot 10^{-10}$
24.62	0.35 ± 0.02	22.53 ± 1.56	$5.57 \cdot 10^{-13}$	$(2.90 \pm 0.18) \cdot 10^{-10}$
25.37	0.37 ± 0.02	22.08 ± 0.61	$5.73 \cdot 10^{-13}$	$(2.98 \pm 0.08) \cdot 10^{-10}$
26.53	0.36 ± 0.02	23.97 ± 1.74	$6.12 \cdot 10^{-13}$	$(3.19 \pm 0.23) \cdot 10^{-10}$
28.73	0.36 ± 0.02	20.53 ± 3.23	$5.15 \cdot 10^{-13}$	$(2.68 \pm 0.40) \cdot 10^{-10}$

Table 0.3. Data obtained testing an input solution of 10^{-1} M of SiO_3^{2-}.

Total time (h)	Flow rate (mL/min)	[U] (ppb)	r_{diss} ($mol \cdot s^{-1}$)	r_{diss} ($mol \cdot s^{-1} \cdot m^{-2}$)
0.00	0.10 ± 0.01	22.48 ± 1.22	$1.49 \cdot 10^{-13}$	$(6.60 \pm 0.34) \cdot 10^{-11}$
0.42	0.10 ± 0.01	23.39 ± 1.64	$1.53 \cdot 10^{-13}$	$(6.76 \pm 0.48) \cdot 10^{-11}$
3.32	0.10 ± 0.01	23.23 ± 0.65	$1.60 \cdot 10^{-13}$	$(7.09 \pm 0.19) \cdot 10^{-11}$
8.08	0.09 ± 0.01	25.24 ± 1.32	$1.59 \cdot 10^{-13}$	$(7.04 \pm 0.36) \cdot 10^{-11}$
24.32	0.09 ± 0.01	21.41 ± 0.64	$1.28 \cdot 10^{-13}$	$(5.66 \pm 0.17) \cdot 10^{-11}$
24.78	0.09 ± 0.01	22.38 ± 0.45	$1.35 \cdot 10^{-13}$	$(5.99 \pm 0.12) \cdot 10^{-11}$
26.95	0.08 ± 0.01	21.53 ± 0.71	$1.22 \cdot 10^{-13}$	$(5.38 \pm 0.19) \cdot 10^{-11}$
31.43	0.09 ± 0.01	20.53 ± 1.27	$1.24 \cdot 10^{-13}$	$(5.47 \pm 0.34) \cdot 10^{-11}$

Table 0.4. Data obtained testing an input solution of 10^{-2} M of SiO_3^{2-}.

Total time (h)	Flow rate (mL/min)	[U] (ppb)	r_{diss} ($mol \cdot s^{-1}$)	r_{diss} ($mol \cdot s^{-1} \cdot m^{-2}$)
0.00	0.06 ± 0.01	37.70 ± 1.25	$1.64 \cdot 10^{-13}$	$(7.24 \pm 0.24) \cdot 10^{-11}$
4.23	0.11 ± 0.01	23.85 ± 2.53	$1.77 \cdot 10^{-13}$	$(7.83 \pm 0.17) \cdot 10^{-11}$
21.47	0.07 ± 0.01	33.10 ± 1.48	$1.72 \cdot 10^{-13}$	$(7.59 \pm 0.34) \cdot 10^{-11}$
22.02	0.07 ± 0.01	30.82 ± 0.55	$1.59 \cdot 10^{-13}$	$(7.02 \pm 0.13) \cdot 10^{-11}$
23.95	0.07 ± 0.01	31.93 ± 0.33	$1.59 \cdot 10^{-13}$	$(7.04 \pm 0.07) \cdot 10^{-11}$
28.73	0.07 ± 0.01	32.10 ± 0.42	$1.62 \cdot 10^{-13}$	$(7.16 \pm 0.08) \cdot 10^{-11}$
70.58	0.04 ± 0.01	46.75 ± 0.1.52	$1.45 \cdot 10^{-13}$	$(6.40 \pm 0.36) \cdot 10^{-11}$

Table 0.5. Data obtained testing an input solution of 10^{-3} M of SiO_3^{2-}.

Total time (h)	Flow rate (mL/min)	[U] (ppb)	r_{diss} ($mol \cdot s^{-1}$)	r_{diss} ($mol \cdot s^{-1} \cdot m^{-2}$)
0.00	0.10 ± 0.01	25.60 ± 0.85	$1.87 \cdot 10^{-13}$	$(8.29 \pm 0.16) \cdot 10^{-11}$
4.23	0.11 ± 0.01	26.10 ± 2.44	$2.01 \cdot 10^{-13}$	$(8.90 \pm 0.57) \cdot 10^{-11}$
21.47	0.08 ± 0.01	34.54 ± 1.28	$1.87 \cdot 10^{-13}$	$(8.29 \pm 0.28) \cdot 10^{-11}$
22.02	0.08± 0.01	33.41 ± 2.37	$1.81 \cdot 10^{-13}$	$(8.02 \pm 0.57) \cdot 10^{-11}$
23.95	0.08 ± 0.01	31.93 ± 1.46	$1.68 \cdot 10^{-13}$	$(7.44 \pm 0.34) \cdot 10^{-11}$
28.73	0.07 ± 0.01	36.25 ± 1.73	$1.73 \cdot 10^{-13}$	$(7.64 \pm 0.36) \cdot 10^{-11}$
70.58	0.06 ± 0.01	41.10 ± 0.89	$1.65 \cdot 10^{-13}$	$(7.32 \pm 0.17) \cdot 10^{-11}$

Table 0.6. Obtained data testing input solutions of $5 \cdot 10^{-3}$ M of CO_3^{2-}.

Total time (h)	Flow rate (mL/min)	[U] (ppb)	r_{diss} ($mol \cdot s^{-1}$)	r_{diss} ($mol \cdot s^{-1} \cdot m^{-2}$)
0.00	0.25 ± 0.02	18.69 ± 0.08	$3.31 \cdot 10^{-13}$	$(2.10 \pm 0.00) \cdot 10^{-10}$
0.87	0.24 ± 0.02	25.06 ± 0.48	$4.27 \cdot 10^{-13}$	$(2.70 \pm 0.5) \cdot 10^{-10}$
2.93	0.23 ± 0.02	22.68 ± 3.51	$3.63 \cdot 10^{-13}$	$(2.30 \pm 0.35) \cdot 10^{-10}$
74.65	0.22 ± 0.02	23.75 ± 0.38	$3.61 \cdot 10^{-13}$	$(2.28 \pm 0.03) \cdot 10^{-10}$
78.58	0.20 ± 0.02	18.01 ± 0.98	$2.51 \cdot 10^{-13}$	$(1.59 \pm 0.08) \cdot 10^{-10}$
96.28	0.18 ± 0.02	25.48 ± 1.64	$3.16 \cdot 10^{-13}$	$(2.00 \pm 0.32) \cdot 10^{-10}$

Table 0.7. Obtained data testing input solutions of $2.5 \cdot 10^{-3}$ M of CO_3^{2-}.

Total time (h)	Flow rate (mL/min)	[U] (ppb)	r_{diss} ($mol \cdot s^{-1}$)	r_{diss} ($mol \cdot s^{-1} \cdot m^{-2}$)
0.00	0.33 ± 0.02	58.16 ± 3.82	$1.34 \cdot 10^{-12}$	$(5.40 \pm 0.35) \cdot 10^{-10}$
0.95	0.33 ± 0.02	55.56 ± 6.78	$1.27 \cdot 10^{-12}$	$(5.11 \pm 0.56) \cdot 10^{-10}$
6.42	0.37 ± 0.02	54.25 ± 3.22	$1.39 \cdot 10^{-12}$	$(5.59 \pm 0.27) \cdot 10^{-10}$
22.58	0.34 ± 0.02	61.73 ± 3.17	$1.47 \cdot 10^{-12}$	$(5.93 \pm 0.31) \cdot 10^{-10}$

23.50	0.33 ± 0.02	56.37 ± 2.87	$1.31 \cdot 10^{-12}$	$(5.26 \pm 0.27) \cdot 10^{-10}$
26.22	0.35 ± 0.02	51.91 ± 3.26	$1.27 \cdot 10^{-12}$	$(5.11 \pm 0.32) \cdot 10^{-10}$
29.42	0.36 ± 0.02	49.61 ± 2.66	$1.25 \cdot 10^{-12}$	$(5.02 \pm 026) \cdot 10^{-10}$
30.25	0.37 ± 0.02	60.30 ± 3.46	$1.55 \cdot 10^{-12}$	$(6.23 \pm 0.35) \cdot 10^{-10}$

Table 0.8. Obtained data testing an input solution of 10^{-3} M of SiO_3^{2-} and $9.15 \cdot 10^{-4}$ M of Ca^{2+}.

Total time (h)	Flow rate (mL/min)	[U] (ppb)	r_{diss} ($mol \cdot s^{-1}$)	r_{diss} ($mol \cdot s^{-1} \cdot m^{-2}$)
0.00	0.25 ± 0.02	3.69 ± 0.14	$6.54 \cdot 10^{-14}$	$(3.41 \pm 0.13) \cdot 10^{-11}$
0.87	0.23 ± 0.02	6.13 ± 0.15	$1.01 \cdot 10^{-13}$	$(5.25 \pm 0.13) \cdot 10^{-11}$
2.93	0.22 ± 0.02	5.44 ± 0.36	$8.54 \cdot 10^{-14}$	$(4.45 \pm 0.30) \cdot 10^{-11}$
74.65	0.19 ± 0.02	4.38 ± 0.08	$5.86 \cdot 10^{-14}$	$(3.05 \pm 0.05) \cdot 10^{-11}$
78.58	0.18 ± 0.02	6.25 ± 0.18	$8.10 \cdot 10^{-14}$	$(4.21 \pm 0.12) \cdot 10^{-11}$
96.28	0.17 ± 0.02	5.19 ± 0.16	$6.26 \cdot 10^{-14}$	$(3.26 \pm 0.10) \cdot 10^{-11}$
97.90	0.17 ± 0.02	5.09 ± 0.13	$6.23 \cdot 10^{-14}$	$(3.24 \pm 0.08) \cdot 10^{-11}$

Table 0.9. obtained testing an input solution of $9.15 \cdot 10^{-4}$ M of Ca^{2+} and $2.5 \cdot 10^{-3}$ M of CO_3^{2-}.

Total time (h)	Flow rate (mL/min)	[U] (ppb)	r_{diss} ($mol \cdot s^{-1}$)	r_{diss} ($mol \cdot s^{-1} \cdot m^{-2}$)
0.00	0.32 ± 0.02	29.18 ± 2.45	$6.48 \cdot 10^{-13}$	$(3.38 \pm 0.63) \cdot 10^{-10}$
0.42	0.32 ± 0.02	25.33 ± 1.45	$5.64 \cdot 10^{-13}$	$(2.94 \pm 0.17) \cdot 10^{-10}$
3.32	0.32 ± 0.02	33.01 ± 3.02	$7.36 \cdot 10^{-13}$	$(3.83 \pm 0.85) \cdot 10^{-10}$
8.08	0.31 ± 0.02	35.10 ± 3.06	$7.67 \cdot 10^{-13}$	$(3.99 \pm 0.88) \cdot 10^{-10}$
24.32	0.54 ± 0.02	21.41 ± 0.89	$8.06 \cdot 10^{-13}$	$(4.19 \pm 0.17) \cdot 10^{-10}$
25.25	0.34 ± 0.02	19.85 ± 2.38	$4.79 \cdot 10^{-13}$	$(2.49 \pm 0.75) \cdot 10^{-10}$
26.95	0.67 ± 0.02	20.62 ± 1.52	$9.63 \cdot 10^{-13}$	$(5.01 \pm 0.37) \cdot 10^{-10}$

Table 0.10. Obtained data testing an input solution of 10^{-1} M of SiO_3^{2-} and $5 \cdot 10^{-3}$ M of CO_3^{2-}.

Total time (h)	Flow rate (mL/min)	[U] (ppb)	r_{diss} ($mol \cdot s^{-1}$)	r_{diss} ($mol \cdot s^{-1} \cdot m^{-2}$)
0.00	0.11 ± 0.01	21.44 ± 1.02	$1.65 \cdot 10^{-13}$	$(1.04 \pm 0.05) \cdot 10^{-10}$
0.42	0.11 ± 0.01	24.38 ±1.11	$1.86 \cdot 10^{-13}$	$(1.17 \pm 0.05) \cdot 10^{-10}$
3.32	0.06 ± 0.01	48.40 ± 3.05	$1.96 \cdot 10^{-13}$	$(1.24 \pm 0.07) \cdot 10^{-10}$
8.08	0.11 ± 0.01	24.34 ± 0.19	$1.93 \cdot 10^{-13}$	$(1.22 \pm 0.01) \cdot 10^{-10}$
24.32	0.10 ± 0.01	30.88 ± 3.96	$2.16 \cdot 10^{-13}$	$(1.37 \pm 0.17) \cdot 10^{-10}$

Table 0.11. Obtained data testing an input solution of 10^{-2} M of SiO_3^{2-} and $5 \cdot 10^{-3}$ M of CO_3^{2-}.

Total time (h)	Flow rate (mL/min)	[U] (ppb)	r_{diss} ($mol \cdot s^{-1}$)	r_{diss} ($mol \cdot s^{-1} \cdot m^{-2}$)
0.00	0.24 ± 0.02	24.56 ± 1.44	$4.20 \cdot 10^{-13}$	$(1.95 \pm 1.14) \cdot 10^{-10}$
41.43	0.12 ± 0.02	33.83 ± 11.7	$2.92 \cdot 10^{-13}$	$(1.36 \pm 0.46) \cdot 10^{-10}$
41.43	0.18 ± 0.02	34.93 ± 6.32	$4.40 \cdot 10^{-13}$	$(2.05 \pm 0.37) \cdot 10^{-10}$
41.90	0.18 ± 0.02	33.25 ± 4.06	$4.24 \cdot 10^{-13}$	$(1.97 \pm 0.24) \cdot 10^{-10}$
44.10	0.15 ± 0.02	30.96 ± 7.22	$3.17 \cdot 10^{-13}$	$(1.47 \pm 0.36) \cdot 10^{-10}$
65.60	0.17 ± 0.02	28.21 ± 3.63	$3.42 \cdot 10^{-13}$	$(1.60 \pm 0.20) \cdot 10^{-10}$
66.13	0.19 ± 0.02	27.09 ± 7.87	$3.57 \cdot 10^{-13}$	$(1.66 \pm 0.47) \cdot 10^{-10}$
68.62	0.19 ± 0.02	23.23 ± 1.61	$3.10 \cdot 10^{-13}$	$(1.44 \pm 0.10) \cdot 10^{-10}$
90.22	0.14 ± 0.02	26.15 ± 0.54	$2.59 \cdot 10^{-13}$	$(1.21 \pm 0.03) \cdot 10^{-10}$
90.97	0.13 ± 0.02	27.19 ± 5.14	$2.56 \cdot 10^{-13}$	$(1.19 \pm 0.31) \cdot 10^{-10}$
92.13	0.13 ± 0.02	36.27 ± 6.25	$3.18 \cdot 10^{-13}$	$(1.48 \pm 0.32) \cdot 10^{-10}$
94.33	0.11 ± 0.02	34.39 ± 2.58	$2.73 \cdot 10^{-13}$	$(1.27 \pm 0.41) \cdot 10^{-10}$

Table 0.12. Obtained data testing an input solution of 10^{-3} M of SiO_3^{2-} and $5 \cdot 10^{-3}$ M of CO_3^{2-}.

Total time (h)	Flow rate (mL/min)	[U] (ppb)	r_{diss} ($mol \cdot s^{-1}$)	r_{diss} ($mol \cdot s^{-1} \cdot m^{-2}$)
0.00	0.18 ± 0.02	18.69 ± 0.28	$2.33 \cdot 10^{-13}$	$(1.03 \pm 0.02) \cdot 10^{-10}$
0.87	0.18 ± 0.02	31.64 ± 0.53	$3.94 \cdot 10^{-13}$	$(1.75 \pm 0.03) \cdot 10^{-10}$
2.93	0.17 ± 0.02	26.69 ± 0.77	$3.18 \cdot 10^{-13}$	$(1.41 \pm 0.04) \cdot 10^{-10}$
74.65	0.21 ± 0.02	22.33 ± 0.62	$3.34 \cdot 10^{-13}$	$(1.48 \pm 0.04) \cdot 10^{-10}$
78.58	0.22 ± 0.02	22.71 ± 0.35	$3.58 \cdot 10^{-13}$	$(1.58 \pm 0.02) \cdot 10^{-10}$
96.28	0.18 ± 0.02	24.95 ± 1.79	$3.10 \cdot 10^{-13}$	$(1.37 \pm 0.09) \cdot 10^{-10}$
97.90	0.18 ± 0.02	26.56 ± 0.27	$3.30 \cdot 10^{-13}$	$(1.46 \pm 0.14) \cdot 10^{-10}$

Table 0.13. Obtained data testing input solutions of 10^{-3}, 10^{-2} and 10^{-1} M of SiO_3^{2-} with $5 \cdot 10^{-3}$ M of CO_3^{2-}.

Total time (h)	Flow rate (mL/min)	[U] (ppb)	r_{diss} ($mol \cdot s^{-1}$)	r_{diss} ($mol \cdot s^{-1} \cdot m^{-2}$)
0	0.43 ± 0.02	27.11 ± 2.35	$8.24 \cdot 10^{-13}$	$(4.29 \pm 0.38) \cdot 10^{-10}$
5.00	0.44 ± 0.02	27.83 ± 2.22	$8.49 \cdot 10^{-13}$	$(4.42 \pm 0.34) \cdot 10^{-10}$
15.00	0.43 ± 0.02	22.64 ± 0.94	$6.78 \cdot 10^{-13}$	$(3.53 \pm 0.14) \cdot 10^{-10}$
29.00	0.41 ± 0.02	22.39 ± 0.15	$6.41 \cdot 10^{-13}$	$(3.34 \pm 0.02) \cdot 10^{-10}$
38.00	0.42 ± 0.02	20.75 ± 0.89	$6.04 \cdot 10^{-13}$	$(3.14 \pm 0.13) \cdot 10^{-10}$
50.00	0.40 ± 0.02	25.96 ± 1.23	$7.24 \cdot 10^{-13}$	$(3.77 \pm 0.17) \cdot 10^{-10}$